

AperTO - Archivio Istituzionale Open Access dell'Università di Torino

**Vancomycin-loaded nanobubbles: A new platform for controlled antibiotic delivery against methicillin-resistant *Staphylococcus aureus* infections**

**This is the author's manuscript**

*Original Citation:*

*Availability:*

This version is available <http://hdl.handle.net/2318/1634018> since 2020-08-31T14:49:44Z

*Published version:*

DOI:10.1016/j.ijpharm.2017.03.033

*Terms of use:*

**Open Access**

Anyone can freely access the full text of works made available as "Open Access". Works made available under a Creative Commons license can be used according to the terms and conditions of said license. Use of all other works requires consent of the right holder (author or publisher) if not exempted from copyright protection by the applicable law.

(Article begins on next page)

Manuscript Number: IJP-D-16-02774R1

Title: Vancomycin-loaded nanobubbles: a new platform for controlled antibiotic delivery against methicillin-resistant *Staphylococcus aureus* infections.

Article Type: Research Paper

Section/Category: Pharmaceutical Nanotechnology

Keywords: nanobubbles, vancomycin, methicillin-resistant *Staphylococcus aureus*, ultrasound, prolonged release

Corresponding Author: Dr. Roberta Cavalli,

Corresponding Author's Institution: University of Turin

First Author: Monica Argenziano

Order of Authors: Monica Argenziano; Giuliana Banche; Anna Luganini; Nicole Finesso; Valeria Allizond; Giulia Rossana Gulino; Amina Khadjavi; Rita Spagnolo; Vivian Tullio; Giuliana Giribaldi; Caterina Guiot; Anna Maria Cuffini; Mauro Prato; Roberta Cavalli

Abstract: Vancomycin (Vm) currently represents the gold standard against methicillin-resistant *Staphylococcus aureus* (MRSA) infections. However, it is associated with low oral bioavailability, formulation stability issues, and severe side effects upon systemic administration. These drawbacks could be overcome by Vm topical administration if properly encapsulated in a nanocarrier. Intriguingly, nanobubbles (NBs) are responsive to physical external stimuli such as ultrasound (US), promoting drug delivery. In this work, perfluoropentane (PFP)-cored NBs were loaded with Vm by coupling to the outer dextran sulfate shell. Vm-loaded NBs (VmLNBS) displayed ~300 nm sizes, anionic surfaces and good drug encapsulation efficiency. In vitro, VmLNBS showed prolonged drug release kinetics, not accompanied by cytotoxicity on human keratinocytes. Interestingly, VmLNBS were generally more effective than Vm alone in MRSA killing, with VmLNB antibacterial activity being more sustained over time as a result of prolonged drug release profile. Besides, VmLNBS were not internalized by staphylococci, opposite to Vm solution. Further US association promoted drug delivery from VmLNBS through an in vitro model of porcine skin. Taken together, these results support the hypothesis that proper Vm encapsulation in US-responsive NBs might be a promising strategy for the topical treatment of MRSA wound infections.

Torino, Italy: 14<sup>th</sup> March 2017

To the Editor  
of the International Journal of Pharmaceutics

Dear Editor,

please find attached here the revised version (both marked and clean copies) of our research article titled “Vancomycin-loaded nanobubbles: a new platform for controlled antibiotic delivery against methicillin-resistant *Staphylococcus aureus* infections”.

As requested, the manuscript was implemented according to the reviewer’s suggestions and all the references were modified according to the journal’s author guidelines. Following the reviewer’s comments, the image quality was improved for all figures. A rebuttal letter containing our replies to the author(s)’s comments is also attached.

We sincerely hope that you will find the revised version of the manuscript acceptable for publication by the International Journal of Pharmaceutics.

We are looking forward to receiving your feedback.

Kind regards

Prof. Roberta Cavalli

## IJP AUTHOR CHECKLIST

Dear Author,

It frequently happens that on receipt of an article for publication, we find that certain elements of the manuscript, or related information, is missing. This is regrettable of course since it means there will be a delay in processing the article while we obtain the missing details.

In order to avoid such delays in the publication of your article, if accepted, could you please run through the list of items below and make sure you have completed the items.

### Overall Manuscript Details

- Is this the final revised version? X
- Are all text pages present? X
- Are the corresponding author's postal address, telephone and fax numbers complete on the manuscript? X
- **Have you provided the corresponding author's e-mail address?** X
- **Manuscript type – please check one of the following:**
  - Full-length article X
  - Review article
  - Rapid Communication
  - Note
  - Letter to the Editor
  - Other
- **Manuscript section – paper to be published in:**
  - Pharmaceutical Nanotechnology section X
  - Personalised Medicine section

### Manuscript elements

- Short summary/abstract enclosed? X
- 3-6 Keywords enclosed? X
- Complete reference list enclosed? X
- Is the reference list in the correct journal style? X
- Are all references cited in the text present in the reference list? X
- Are all **original** figures cited in the text enclosed? X
  - Electronic artwork format? -----
- Are figure legends supplied? X
- Are all figures numbered and orientation provided? X
- Are any figures to be printed in colour? 
  - If yes, please list which figures here:-----
- If applicable, are you prepared to pay for reproduction in colour?
- Are all tables cited in the text supplied? X

### General

- Can you accept pdf proofs sent via e-mail? X

**Reviewers' comments:**

**Reviewer #1: Comments:**

1. The quality of figures should be greatly improved, especially the graphical abstract, Figure 3 and 6.

We apologize for such an issue. According to the reviewer's suggestion, the image quality was improved for all figures.

2. In line 159, the section 2.2.1., How many ml of dextran sulfate aqueous solutions were added into the Vm solution? What is the solvent of Vm solution? Water or other organic solvents? When centrifuge the unbound Vm, how much is the centrifugal speed? And the centrifugal time also should be provided.

One ml of dextran sulfate aqueous solution at increasing concentrations was added into 1 ml of vancomycin aqueous solution. The centrifugal speed used was 20000 rpm for 15 minutes. The manuscript was implemented with such information (Materials&Methods section, par. 2.2.1).

3. For preparing pre-emulsion containing Epikuron® 200, palmitic acid and PFP, how much g/mg of PFP was used? To prepare polymeric NBs, How many ml of dextran sulfate aqueous solution was added into the PFP emulsion?

The amount of PFP and dextran sulfate used for each nanobubble formulation were 500  $\mu$ L and 350  $\mu$ L, respectively. Such information was added in the text (Materials&Methods section, par. 2.2.2).

4. In line 199, for the TEM observation, the type and brand for the TEM equipment should be provided in the text.

The type and brand of the instrument used for TEM analyses (Philips CM10 (Eindhoven, NL)) were added in the text (Materials&Methods section, par. 2.3.1).

5. To measure the loading capacity, the VmLNBS solution was sonicated and centrifuged, and then the supernatant was analyzed. How to validate the VmLNBS were completely broken? Why not use the organic solvent to destroy the structure of the VmLNBS?

The parameters of the used freeze-drying process are severe to maintain the integrity of the nanostructure in the absence of any cryoprotectors. Preliminary experiments were carried out to evaluate by optical microscopy the nanobubble structure and to set a protocol suitable for determining the loading capacity. The manuscript was modified accordingly (Materials&Methods section, par. 2.3.5).

6. In line 285, the unit of centrifugal speed was g, in line 230, the unit is rpm. The author should check them. Some similar expressions also should be uniformed, such as mL and microL.

All units of centrifugal speed as well as those indicating microliters were uniformed throughout the full text.

7. The viscosity of VmLNBS was higher than that of NB. The reason should be explained in the section of "Discussion". Does the change of viscosity affect loading capacity, encapsulation efficiency, physical stability, Vm release, and permeation efficiency?

We apologize for the typing mistake concerning the viscosity value of blank NB formulations. We determined again the viscosity using the Ubbelohde capillary viscosimeter to confirm the data. The viscosity of all NB formulations (i.e. blank NBs, VmLNBS, fluorescent NBs, and fluorescent VmLNBS) did not show any significant changes. A specific sentence was added in the text (Results section par. 3.1).

8. Table 2 can be incorporated in Table 1.

According to the reviewer's suggestion, Table 2 was incorporated in Table1.

**Reviewer #2:** The development of novel systems for antibiotics is in its infancy as compared to other disease conditions and is receiving increasing interest in the literature. Whilst several nanosystems are being reported for vancomycin, few, if any have been with nanobubbles. Further, transdermal delivery of nanoencapsulated antibiotics is an emerging research area. This paper describes the encapsulation of vancomycin into nanobubbles for ultrasound mediated drug release and also to bypass the stratum corneum to optimize the treatment of wound infections. This proof of concept study is well designed and the potential of this delivery system is demonstrated. The paper is well written with some minor recommendations:

1. Images of the nanobubbles show one with a single nanobubble and another with 2. Ideally an image showing a population representation should be considered.

A TEM image showing a population representation of VmLNBS was added in the Supplementary Information.

2. There are several inconsistencies in the referencing style which need to be corrected.

All the references were modified according to the journal's author guidelines.

3. Pg 18, Line 368. The last sentence is incorrect and needs to be rewritten.

According to the reviewer's suggestion, we changed the sentence as follows: "As shown in Figure 3, the drug resulted much more stable from a chemical point of view when properly incorporated in the nanocarrier (VmLNBS) than as such in solution." (Results section, par. 3.2)

**Reviewer #3:** Manuscript IJP-D-16-02774 "Vancomycin - loaded nanobubbles: a new platform for controlled..." by Argenziano et al. describes the fabrication, characterization and release capability of polymer shelled droplets loaded with vancomycin.

The manuscript should be implemented according to the following comments:

1) It should be specified whether PFP is liquid.

Perfluoropentane is a perfluorocarbon with a boiling point of 29°C, hence liquid at room temperature. The use of PFP allows liquid droplet generation at room temperature. Then, PFP in nanodroplets can be activated by an external stimulus, like ultrasound, by means of a mechanism called acoustic droplet vaporization, causing the droplet to become a bubble. The sentence was added in the manuscript (Introduction section, lines 117-120).

2) Term "nanobubbles" can be misleading. At room temperature the core of the particles is liquid PFP. Therefore nanobubbles does not describes correctly such particles. It would be more proper the term "nanodroplets" or "nanovesicles"

The formulation is referred to as "nanobubbles" for sake of simplicity (to distinguish them from so-called decafluoropentane-containing nanodroplets, already patented by our group; see Introduction section for more details about those nanodroplets) but we acknowledge that, prior to the application of ultrasound, it would be more precise to use the term "nanodroplets" when the core is constituted of perfluoropentane. This clarification was included in the text (Introduction section, lines 129-132).

3) Figures are not numbered and are very low in resolution (including the graphical abstract). Sometimes they are not readable.

We apologize for the low quality of figures. According to the reviewer's suggestion, the resolution of all figures was improved. Also, Figures were numbered in accordance to legend numbers.

4) Scheme of the particle differs from the particle description of the graphical abstract in the position of vancomycin, tethered to the external surface of the particle and in the particle shell, respectively.

Vancomycin is included in the polysaccharide shell. For clarity, we modified Figure 1.

5) Viscosity measurements obtained by capillary viscosimetry should be defined. With an Ubbelohde capillary viscometer a relative viscosity, a specific viscosity, an intrinsic viscosity can be obtained. Which one is reported ? All of them have different dimensions from the reported one, i.e. cP. Relative (to solvent) and specific viscosities are dimensionless, intrinsic viscosity has dimension of an inverse of concentration.

With the Ubbelohde capillary viscometer, the time required for the nanosuspension to flow through a capillary of a known diameter of a certain factor (K) between two marked points was measured. By multiplying the time taken, by the factor of the viscometer (0.105), the kinematic viscosity was obtained. The dynamic viscosity was obtained by multiplying kinematic viscosity by density. The cP is the unit of dynamic viscosity in the metric CGS (centimeter-gram-second) system.

6) Vancomycin permeation study puzzled me a lot. The experiment should be conducted at osmotic conditions. To avoid Donnan effects with a charged not diffusible solute, i.e. nanobubbles, a suitable diffusible ionic strength should be used on both the compartments separated by the membrane. According to the given description NaCl 0.9 % w/w has been added only on one compartment. In this conditions other, not controlled contributions affects the diffusion process of vancomycin. In the description of the set up, the concentration of nanobubbles is not reported.

We apologize for the inaccurate description of the experimental setup. For *in vitro* permeation studies, NB samples were prepared in saline solution (NaCl 0.9% w/v). The concentration of NBs in the donor phase was  $1 \times 10^{12}$  NBs/ml. All information was added to the text (Materials&Methods section, par. 2.2.2 and 2.5).

7) When ultrasound are applied, it is important to check the behaviour of the "nanobubbles" (nanodroplets) in order to frame the enhanced release. Do "nanobubbles" (nanodroplets) undergo acoustic droplet vaporization? This effect is known to transform droplets into bubbles, thus changing the release of the payload.

Nanobubbles were observed by US standard imaging (MyLab ESAOTE instrument) and they showed a good scattering response, either in the absence or presence of vancomycin. Further investigations are needed to check whether actual vaporization occurred. With regard to the drug release, preliminary experiments showed an enhanced release kinetics after US application.

8) Pg 6 line 115: PFP is liquid or gas ?

Perfluoropentane is liquid at room temperature, having a boiling point of about 29 °C. Therefore, it is gaseous at body temperature (37°C) as such.

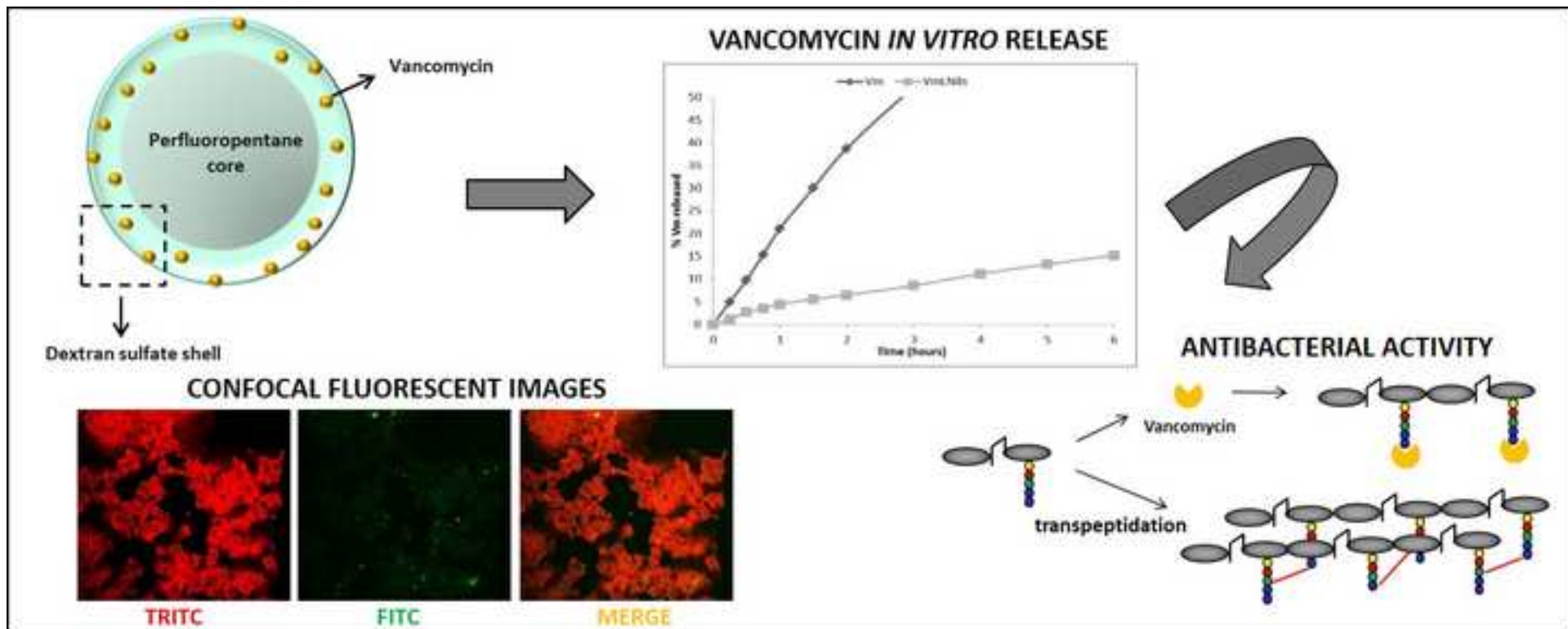
9) Pg 15 line 332: why in confocal microscopy imaging, bacteria are dried ?

The drying of bacteria is a step necessary for their staining. After smearing of bacteria on the glass-slide, every staining procedure considers that bacteria have to be air-dried to fix them on the slide and to avoid the subsequent rinsing of the smear during staining procedure, as well as to allow the sample to more readily take up stain(s).

10) Vancomycin hydrochloride is not mentioned in the Material section.

Vancomycin hydrochloride was from Sigma-Aldrich (St Louis, MO). Therefore, it falls into the general sentence "All materials were from Sigma-Aldrich, St Louis, MO, unless those indicated as follows" (first sentence of par. 2.1 in Materials&Methods section).





1 **Vancomycin-loaded nanobubbles: a new platform for controlled antibiotic delivery against**  
2 **methicillin-resistant *Staphylococcus aureus* infections.**

3

4 Monica Argenziano<sup>1</sup>, Giuliana Banche<sup>2,\*</sup>, Anna Luganini<sup>3</sup>, Nicole Finesso<sup>4</sup>, Valeria Allizond<sup>2</sup>, Giulia  
5 Rossana Gulino<sup>4</sup>, Amina Khadjavi<sup>4,5</sup>, Rita Spagnolo<sup>1</sup>, Vivian Tullio<sup>2</sup>, Giuliana Giribaldi<sup>4</sup>, Caterina  
6 Guiot<sup>5</sup>, Anna Maria Cuffini<sup>2</sup>, Mauro Prato<sup>2,5,§</sup>, Roberta Cavalli<sup>1, §,\*</sup>

7

8 <sup>1</sup> *Dipartimento di Scienza e Tecnologia del Farmaco, Università degli Studi di Torino, Torino, Italy*

9 <sup>2</sup> *Dipartimento di Scienze della Sanità Pubblica e Pediatriche, Università degli Studi di Torino, Torino,*  
10 *Italy*

11 <sup>3</sup> *Dipartimento di Scienze della Vita e Biologia dei Sistemi, Università degli Studi di Torino, Torino,*  
12 *Italy*

13 <sup>4</sup> *Dipartimento di Oncologia, Università degli Studi di Torino, Torino, Italy*

14 <sup>5</sup> *Dipartimento di Neuroscienze, Università degli Studi di Torino, Torino, Italy*

15 *§ Equal contribution to the work*

16 *\* Corresponding authors:*

17 Prof. Roberta Cavalli, Dipartimento di Scienza e Tecnologia del Farmaco, Università degli Studi di  
18 Torino, via P. Giuria 9, 10125 Torino, Italy. Phone no.: +39-011-6707686. Fax no.: +39-011-6707687.  
19 E-mail address: [roberta.cavalli@unito.it](mailto:roberta.cavalli@unito.it)

20 Dr. Giuliana Banche, Dipartimento di Scienze della Sanità Pubblica e Pediatriche, Università degli  
21 Studi di Torino, Via Santena 9, 10126 Torino, Italy. Phone no.: +39-011-6705627. Fax no.: +39-011-  
22 2365627. E-mail address: [giuliana.banche@unito.it](mailto:giuliana.banche@unito.it)

23 **Abstract**

24

25 Vancomycin (Vm) currently represents the gold standard against methicillin-resistant *Staphylococcus*  
26 *aureus* (MRSA) infections. However, it is associated with low oral bioavailability, formulation stability  
27 issues, and severe side effects upon systemic administration. These drawbacks could be overcome by  
28 Vm topical administration if properly encapsulated in a nanocarrier. Intriguingly, nanobubbles (NBs)  
29 are responsive to physical external stimuli such as ultrasound (US), promoting drug delivery. In this  
30 work, perfluoropentane (PFP)-cored NBs were loaded with Vm by coupling to the outer dextran sulfate  
31 shell. Vm-loaded NBs (VmLNBS) displayed ~300 nm sizes, anionic surfaces and good drug  
32 encapsulation efficiency. *In vitro*, VmLNBS showed prolonged drug release kinetics, not accompanied  
33 by cytotoxicity on human keratinocytes. Interestingly, VmLNBS were generally more effective than  
34 Vm alone in MRSA killing, with VmLNB antibacterial activity being more sustained over time as a  
35 result of prolonged drug release profile. Besides, VmLNBS were not internalized by *staphylococci*,  
36 opposite to Vm solution. Further US association promoted drug delivery from VmLNBS through an *in*  
37 *vitro* model of porcine skin. Taken together, these results support the hypothesis that proper Vm  
38 encapsulation in US-responsive NBs might be a promising strategy for the topical treatment of MRSA  
39 wound infections.

40

41 **Key words**

42 Nanobubbles; vancomycin; methicillin-resistant *Staphylococcus aureus*; ultrasound; prolonged release.

43

44

45

46

## 47 **1. Introduction**

48

49 Chronic wounds fail to proceed through timely regulated and interrelated processes to restore  
50 anatomical and functional integrity of the injured tissues (Lazarus et al., 1994) such as diabetic feet,  
51 bedsores, and venous ulcers (Markova et al., 2012). To date, these types of wounds are considered like  
52 a silent epidemic, affecting a large fraction of the world population and posing a major gathering threat  
53 to the public health and economy of all developed countries (Daeschlein, 2013). Hospitalized patients  
54 are at particular risk, especially those suffering from diabetes, human immunodeficiency virus or other  
55 immune disorders, as well as those undergoing chemotherapy (Payne et al., 2008).

56 Beyond delayed healing processes due to different factors (hypoxia, persistent inflammation, and  
57 altered balances between tissue remodelling proteinases and their inhibitors), chronic wounds are often  
58 worsened by microbial infections (Gurusamy et al., 2013). Among the bacteria responsible for skin  
59 infection, *Staphylococcus aureus* represents the most common pathogen to be identified in chronic  
60 wounds, with methicillin-resistant *S. aureus* (MRSA) accounting for upward of 20% to 50% of cases  
61 (Price, 2010). MRSA colonies often develop at the interface between synthetic prostheses and  
62 biological tissues, particularly during surgery and post-surgery course. In addition, MRSA colonization  
63 or infection of wounds can result in MRSA bacteremia, which is associated with a 30-day mortality of  
64 about 28% to 38% patients (Gurusamy et al., 2013).

65 The main goal of chronic wound treatment is to decrease the injuring-associated microbial load, thus  
66 allowing wound healing processes to take place. However, conventional systemic delivery of  
67 antibiotics not only entails poor penetration into ischemic and necrotic tissues, but can also cause  
68 systemic toxicity with associated renal and liver complications, resulting in forced hospitalization for  
69 further monitoring and advanced treatment. On the contrary, topically applied antimicrobials have  
70 proven effective in decreasing bacterial levels in granulating wounds (Diehr et al., 2008). Therefore,

71 alternative local delivery of antimicrobials - either by topical administration or through novel delivery  
72 devices - may enable to keep high local antibiotic concentrations for prolonged release times without  
73 reaching systemic toxicity (Zilberman et al., 2008).

74 A promising approach to develop a topical therapy for microbial infection in skin and soft tissues  
75 would employ biocompatible nanomaterials and drug nanocarriers. Indeed, nanotechnology represents  
76 an emerging field to be exploited for antibiotic drug delivery. Thanks to their physical and chemical  
77 properties (small size, high surface-to-volume ratio and suitable surface modification) nano-sized  
78 materials may be used as drug carriers to trespass several physiological barriers and to reach biological  
79 targets. The coupling of nanocarriers with anti-infectious agents makes it likely to increase drug  
80 concentrations and drug penetration at the site of infection. As a result, it might not only improve the  
81 therapeutic index but also reduce some issues associated with nonspecific cytotoxicity and antibiotic  
82 resistance (Sharma et al., 2012).

83 Vancomycin hydrochloride, being effective against many Gram-positive bacteria that are unresponsive  
84 to common antibiotics, represents the gold standard against MRSA infections (Kullar et al., 2016).  
85 However, Vm is poorly absorbed from the gastrointestinal tract with a low oral bioavailability. Low  
86 intravenous infusion is often suggested as a feasible alternative for drug administration, but Vm  
87 instability in aqueous solutions at 37°C could imply a tremendous reduction of drug effectiveness  
88 (Mawhinney et al., 1992; Raverdy et al., 2013). Following parenteral administration, Vm displays a  
89 slow mode of action, a complex concentration-time profile, and a disappointingly low penetration in  
90 tissues (Vandecasteele et al., 2012). Furthermore, systemic Vm administration can be associated with  
91 several adverse effects (Vidal et al., 1992). On the other hand, Vm topical application – that would be  
92 much safer than systemic administration - is currently limited by several factors such as skin barrier  
93 properties and poor drug permeability (Giandalia et al., 2001). Being the main goal of chronic wound  
94 treatment to decrease the microbial load, allowing the healing processes to take place, new delivery

95 protocol should be devised, since conventional systemic delivery of antibiotics requires a drug  
96 concentration which is locally ineffective because of the poor penetration into ischemic and necrotic  
97 tissues, but can cause systemic toxicity and topically applied antimicrobials have proven effective in  
98 decreasing bacterial levels in granulating wounds (Diehr et al., 2007), without inducing systemic  
99 toxicity (Zilberman et al., 2008) but suffer from poor diffusion across membranes.

100 Intriguingly, the use of a nanocarrier may help to avoid the abovementioned drawbacks. Notably,  
101 nanocarriers such as liposomes, microemulsions, and lipid nanoparticles have the potential to deliver  
102 drugs to the skin more efficiently than conventional topical carriers such as creams and ointments, that  
103 are not usually recommended for applications on injured skin (Giandalia et al., 2001; Prabhu et al.,  
104 2012). However, the response to drug topical applications has been too weak so far, mainly due to the  
105 inability to cross the external skin barrier (*stratum corneum*) and reach the dermal regions where the  
106 bacteria are nested. Interestingly, physical media such as ultrasound (US) are reportedly able to trigger  
107 drug release at the site of infection by temporarily increasing skin permeability through sonophoresis.  
108 As such, US is useful to promote drug targeting and transdermal delivery in a non-invasive manner  
109 (Azagury et al., 2014; Park et al, 2012).

110 Microbubbles (MBs) (Guiot et al., 2006), nanobubbles (NBs) (Cavalli et al., 2009a; Cavalli et al.,  
111 2009b; Cavalli et al., 2016) and nanodroplets (NDs) (Magnetto et al., 2014; Prato et al., 2015) are  
112 suitable carriers to be combined with such a physical trigger. They are spherical core-shell structures  
113 filled with gases such as perfluorocarbons. Particularly, oxygen-cored nanostructures can be employed  
114 both for sonography (as contrast agents) (Fokong et al., 2012; Marxer et al., 2011) and for therapy (as  
115 hypoxia- and infection-counteracting devices) (Gulino et al., 2015; Banche et al., 2015; Khadjavi et al.,  
116 2015; Basilico et al., 2015; Prato et al., 2016). In particular NBs, consisting in an outer shell of a  
117 biocompatible/biodegradable polysaccharide (chitosan, dextran, or dextran sulfate) and an inner core  
118 filled with an oxygen-storing fluorocarbon (perfluoropentane, PFP), have been purposely developed as

119 a new non-invasive, low-cost and multipurpose nanotechnological platform (Cavalli et al., 2009a;  
120 Cavalli et al., 2009b; Cavalli et al., 2016). PFP is a perfluorocarbon with a boiling point of 29°C, hence  
121 liquid at room temperature. The use of PFP allows liquid droplet generation at room temperature. Then,  
122 PFP in nanodroplets can be activated by an external stimulus, like US, by means of a mechanism called  
123 acoustic droplet vaporization, causing the droplet to become a bubble. Depending on the properties of  
124 the nanostructure, NBs can be subsequently coupled with different molecules, such as drugs or genetic  
125 materials, thus acting as nanocarriers (Cavalli et al., 2012; Cavalli et al., 2013; Delalande et al., 2012;  
126 Yin et al., 2014). Due to their structure and their gaseous core, NBs are very responsive to US and can  
127 take advantage from a number of effects related to microcavitation and microstreaming, occurring at  
128 the liquid-membrane interface and responsible for transitory and reversible openings of the pores, thus  
129 crossing the membrane itself and delivering their content beyond the tissue (sonophoresis) or the cell  
130 (sonoporation) membrane (Karshafian et al., 2009).

131 Based on these preconditions, the present work aimed at producing dextran sulfate-shelled and PFP-  
132 cored NBs for Vm local delivery to potentially treat skin infectious diseases. The formulation is  
133 referred to as “nanobubbles” for sake of simplicity but it must be said that, prior to the application of  
134 US, it would be more accurate to use the term “nanodroplets” when the core is constituted of PFP.  
135 Therefore, Vm-loaded NBs (VmLNBs) were prepared and characterized for physico-chemical  
136 parameters and drug release kinetics; tested for biocompatibility with human skin cells and for their  
137 antibacterial properties or interactions with MRSA; and challenged for responsiveness to US, in order  
138 to assess their effectiveness as Vm nanocarriers for local delivery.

139

140 **2. Material and methods**

141

142 **2.1. Materials**

143 All materials were from Sigma-Aldrich, St Louis, MO, unless those indicated as follows. Sterile  
144 plastics were from Costar, Cambridge, UK; ethanol (96%) was from Carlo Erba (Milan, Italy); soybean  
145 lecithin (Epikuron 200<sup>®</sup>) was from Cargill (Hamburg, Germany); 1-800 Millipore system to obtain  
146 ultrapure water and Amicon<sup>®</sup> Ultra-0.5 centrifugal filter device were from Millipore (Molsheim,  
147 France); Ultra-Turrax SG215 homogenizer was from IKA (Staufen, Germany); RPMI 1640 medium  
148 was from Invitrogen (Carlsbad, CA); Nanobrook 90Plus Particle Size Analyzer was from Brookhaven  
149 (New York City, NY); Philips CM10 electron microscope was from Philips (Eindhoven, the  
150 Netherlands); Ubbelohde capillary viscosimeter was from SCHOTT Instruments GmbH (Mainz,  
151 Germany); Perkin Elmer PUMP 250B was from Perkin Elmer (Waltham, MA); Flexar UV/Vis LC  
152 spectrophotometer detector was from Perkin Elmer (Waltham, MA); Agilent TC C<sub>18</sub> columns were  
153 from Agilent (Santa Clara, CA); Orion Model 420A pH Meter was from Thermo Scientific (Waltham,  
154 MA); Semi-Micro Osmometer K-7400 was from Knauer (Berlin, Germany); Beckman Coulter Allegra  
155 64R Centrifuge was from Beckman Coulter (Brea, CA); Spectra/Por cellulose membranes were from  
156 Spectrum Laboratories (Rancho Dominguez, CA); HaCaT cells were from Cell Line Service GmbH  
157 (Eppelheim, Germany); cell culture RPMI 1640 and Dulbecco's modified Eagle's medium (DMEM)  
158 were from Invitrogen (Carlsbad, CA); streptomycin was from Cambrex Bio Science (Vervies,  
159 Belgium); humidified CO<sub>2</sub>/air-incubator was from Thermo Fisher Scientific Inc. (Waltham, MA);  
160 tryptic soy broth (TSB) and tryptic soy agar (TSA) were from Merk KgaA (Darmstadt, Germany);  
161 Olympus Fluoview 200 laser scanning confocal system mounted on an inverted IX70 Olympus  
162 microscope was from Olympus America Inc. (Melville, NY, USA) ; SPSS 16.0 software was from  
163 SPSS Inc. (Chicago, IL).



## 164 **2.2. Development and manufacturing of formulations**

165

### 166 ***2.2.1. Determination of Vm and dextran sulfate interaction ratio***

167 Increasing concentrations (0.25, 0.5, 1.0, 2.0 mg/mL) of dextran sulfate aqueous solutions (1 mL) were  
168 added to 1 mL of Vm aqueous solution (1 mg/mL) under magnetic stirring at room temperature  
169 overnight. After equilibration, the systems were separated by centrifugation (20000 rpm, 15 minutes)  
170 using a centrifugal filter device (Amicon<sup>®</sup> Ultra), in order to determine the amount of unbound Vm in  
171 the filtrate phase. The drug concentration in the filtrate was determined using the HPLC method  
172 described below.

173

### 174 ***2.2.2. Preparation of NB, Vm, and VmLNB formulations***

175 NBs were formulated using PFP for the inner core and dextran sulfate for the shell. A purposely tuned  
176 multi-step protocol was designed. Briefly, a pre-emulsion was obtained adding 300  $\mu$ L of an ethanol  
177 solution containing Epikuron<sup>®</sup> 200 and palmitic acid (1% w/v) to 500  $\mu$ L of PFP under magnetic  
178 stirring. After the addition of 4.8 mL of ultrapure water, the system was homogenized using a Ultra-  
179 Turrax SG215 homogenizer. To obtain the polymeric NBs, 350  $\mu$ L of 1% w/v dextran sulfate  
180 (molecular weight = 100 kDa) aqueous solution was added drop-wise under magnetic stirring. Blank  
181 NBs obtained according to this procedure were employed as control formulations in the subsequent  
182 experiments. On the other hand, to obtain VmLNBs, an extra step based on drop-wise addition of a Vm  
183 aqueous solution (pH 3.5) to the so-formed NBs was performed under mild stirring. Different  
184 concentrations of Vm solutions were added to prepare a series of VmLNB formulations with increasing  
185 drug content (0.004, 0.01, 0.1, and 1 mg/mL). VmLNBs were then purified by dialysis to eliminate  
186 unbound molecules. For selected experiments, fluorescent NBs and VmLNBs were obtained by the

187 addition of 6-coumarin (1 mg/mL) to the PFP core. Alternatively, fluorescent Vm was synthesized  
188 through reaction between fluorescein isothiocyanate (FITC) and Vm. For this purpose, an amount of  
189 FITC solution in methanol (0.2 % w/v) was added to Vm aqueous solution and incubated under stirring  
190 overnight in the dark. **Figure 1** shows a representative scheme resuming the general structure of  
191 fluorescent VmLNBS. For cell experiments, NBs were prepared in phosphate buffer saline pH 7.4  
192 (PBS). For *in vitro* permeation studies, NBs were prepared in saline solution (NaCl 0.9% w/v).

193

### 194 **2.2.3. NB sterilization**

195 Firstly, the glassware and the components were sterilized at 121 °C and 2 bar. Subsequently, all NB  
196 formulations were sterilized through UV-C exposure for 20 min. Thereafter, UV-C-treated materials  
197 were incubated with cell culture RPMI 1640 medium in a humidified CO<sub>2</sub>/air-incubator at 37°C up to  
198 72 h, not displaying any signs of microbial contamination when checked by optical microscopy.

199

## 200 **2.3. Characterization of formulations**

201

### 202 **2.3.1. Characterization of NB and VmLNB formulations**

203 The average diameter, polydispersity index and zeta potential were determined by photocalibration  
204 spectroscopy using a particle size analyzer at a scattering angle of 90° and a temperature of 25 °C. NB  
205 suspensions were diluted in deionized filtered water before measurement. For zeta potential  
206 determination, samples of diluted NB formulations were placed in the electrophoretic cell, where an  
207 electric field of approximately 15 V/cm was applied. The morphology of formulations was evaluated  
208 by Transmission Electron Microscopy (TEM), using a Philips CM10 (Eindhoven, NL) instrument. NB  
209 and VmLNB aqueous suspensions were sprayed on Formvar-coated copper grid and air-dried before

210 observation. The viscosity of the samples was determined at 25 °C using a Ubbelohde capillary  
211 viscosimeter.

212

### 213 **2.3.2. HPLC quantitative Vm determination**

214 Vm quantitative determination was carried out by using an HPLC system based on a Perkin Elmer  
215 pump equipped with a spectrophotometer detector. Analyses were performed using an Agilent TC C<sub>18</sub>  
216 column (250 mm × 4.6 mm, 5 µm). The mobile phase was a mixture of KH<sub>2</sub>PO<sub>4</sub> 50 mM (pH 4) and  
217 acetonitrile (92:8 v/v), degassed and pumped through the column with a flow rate of 1 mL/min.  
218 Ultraviolet detection was set at 286 nm. The external standard method was used to calculate the drug  
219 concentration. For this purpose, 1 mg of Vm was weighted, placed in a volumetric flask, and dissolved  
220 in water to obtain a stock standard solution. This solution was then diluted using the mobile phase,  
221 providing a series of calibration solutions, subsequently injected into the HPLC system. Linear  
222 calibration curve was obtained over the concentration range of 0.5–25 µg/mL, with a regression  
223 coefficient of 0.999.

224

### 225 **2.3.3. In vitro evaluation of Vm stability**

226 Vm chemical stability - either solved in aqueous solution or loaded in VmLNBS - was evaluated at  
227 room temperature and at 37 °C over time. A quantitative determination of Vm concentration over time  
228 was carried out using the HPLC method described above.

229

### 230 **2.3.4. NB stability over time and after US administration**

231 The physical stability of NBs was evaluated by morphological analysis and by size and zeta potential  
232 determination of formulation over time. Their average diameters, zeta potential values and morphology  
233 were assessed up to six months. Stability was also investigated following NB exposure to US ( $f = 2.5 \pm$

234 0.1 MHz; t = 10 min; P = 5 W). NB morphology was observed by TEM to confirm the integrity of NB  
235 structure.

236

### 237 **2.3.5. Encapsulation efficiency and loading capacity of Vm in NBs**

238 The encapsulation efficiency of VmLNBS was determined using a centrifugal filter system. 150 µL of  
239 VmLNB suspension were put in an Amicon® Ultra-0.5 centrifugal filter device and centrifuged at  
240 15000 rpm for 30 minutes using Beckman Coulter Allegra 64R Centrifuge. The solution filtered in the  
241 bottom of the tube was quantified and after suitable dilution was analyzed by HPLC, in order to obtain  
242 the concentration of free Vm in VmLNBS suspensions. The encapsulation efficiency was calculated by  
243 subtracting the amount of free drug from the initial amount of added Vm, according to the following  
244 equation:

$$245 \text{ Encapsulation efficiency} = \frac{(\text{total Vm} - \text{free Vm})}{\text{total Vm}} \times 100$$

246 The loading capacity was determined on freeze-dried NB samples. Briefly, a weighted amount of  
247 freeze-dried VmLNBS was suspended in 10 mL of water. After sonication and centrifugation, the  
248 supernatant was diluted with mobile phase and analyzed by HPLC. The loading capacity of Vm in  
249 VmLNBS was calculated as follows:

$$250 \text{ Loading capacity} = \frac{(\text{total Vm} - \text{free Vm})}{\text{NB weight}} \times 100$$

251

### 252 **2.4. In vitro release studies**

253 *In vitro* drug release experiments were conducted in a multi-compartment rotating cell, comprising a  
254 donor chamber separated by a cellulose membrane (cut-off = 12000 Da) from a receiving compartment.

255 One ml of VmLNB suspension at different concentrations (1, 0.1, 0.01 and 0.004 mg/mL) was placed

256 in the donor chamber. The *in vitro* release kinetics of Vm from VmLNB was compared to a Vm  
257 aqueous solution (1 mg/mL) as a control. The receiving phase, containing phosphate buffer 0.05 M (pH  
258 7.4) was withdrawn at regular intervals and replaced with the same amount of fresh buffer. Quantitative  
259 determination of Vm in the withdrawn samples was carried out by the HPLC method, as described in  
260 the previous paragraph. Data were expressed as % of Vm released over time.

261

## 262 **2.5. *In vitro* permeation study**

263 *In vitro* studies were performed using a vertical diffusion Franz cell to evaluate Vm permeation  
264 throughout the skin. The Franz cell consists of a donor compartment, with Vm (1 mg/mL, either free or  
265 carried by VmLNBs,  $1 \times 10^{12}$  NBs/ml) and a receiving compartment containing 0.9% w/w NaCl saline  
266 solution. To simulate the *stratum corneum* properties a membrane pig ear skin was used. Skin slices  
267 were isolated with a dermatome from the outer side of pig ears, obtained from a local slaughterhouse,  
268 and then were frozen at  $-18$  °C. Before starting the experiments, the skin was equilibrated in NaCl 0.9  
269 % w/w saline solution, in the presence of 0.01% sodium azide to preserve the skin, at 25 °C for 30 min.  
270 Then, after washing with saline solution, the skin layer was inserted between the two compartments of  
271 the Franz cell, with the stratum corneum side facing towards the donor chamber. The study was carried  
272 out for 24 hours and the receiving phase was withdrawn at regular times and replaced with the same  
273 amount of fresh receiving medium. The collected samples were then analyzed by HPLC to determine  
274 the amount of Vm permeated over time. US abilities to promote Vm permeation were also investigated.  
275 For this purpose, a high frequency US transducer ( $f = 2.5$  MHz;  $P = 5$  W;  $t = 10$  min) was combined to  
276 a purposely modified vertical diffusion cell. Drug permeation through pig skin after US application was  
277 monitored by HPLC analysis of the cumulative amount of antibiotic reaching the receiving phase over  
278 time.

279

## 280 **2.6. Human biocompatibility studies**

281

### 282 **2.6.1. Human keratinocyte cell cultures**

283 HaCaT, a long-term cell line of human keratinocytes immortalized from a 62-year old Caucasian male  
284 donor (Boukamp et al., 1988), was used for the assessment of Vm and VmLNB biocompatibility. Cells  
285 were grown as adherent monolayers in DMEM medium supplemented with 10% fetal bovine serum,  
286 100 U/mL penicillin, 100 µg/mL streptomycin and 2 mM L-glutamine in a humidified CO<sub>2</sub>/air-  
287 incubator at 37°C. Before starting the experiments, cells were washed with PBS, detached with  
288 trypsin/ethylenediaminetetraacetic acid (0.05/0.02 % v/v), washed with fresh medium and plated at a  
289 standard density (10<sup>6</sup> cells/well in 6-well plates) in 2 mL of fresh medium.

290

### 291 **2.6.2. Vm and VmLNB cytotoxicity**

292 The potential cytotoxic effects of VmLNBS were measured as the release of lactate dehydrogenase  
293 (LDH) from HaCaT cells into the extracellular medium. Briefly, cells were incubated in DMEM  
294 medium for 24 h with/without 1 mg/mL Vm, either free or carried by VmLNBS, in a humidified  
295 CO<sub>2</sub>/air-incubator at 37°C. Then, 1 mL of cell supernatants was collected and centrifuged at 12000 rpm  
296 for 2 min. Cells were washed with fresh medium, detached with trypsin/ethylenediaminetetraacetic acid  
297 (0.05/0.02 % v/v), washed with PBS, resuspended in 1 mL of TRAP (82.3 mM triethanolamine, pH  
298 7.6), and sonicated on ice with a 10 s burst. 5 µL of cell lysates and 50 µL of cell supernatants were  
299 diluted with TRAP and supplemented with 0.5 mM sodium pyruvate and 0.25 mM NADH (300 µL as a  
300 final volume) to start the reaction. The reaction was followed measuring the absorbance at 340 nm (37  
301 °C) with Synergy HT microplate reader. Both intracellular and extracellular enzyme activities were

302 expressed as  $\mu\text{mol}$  of oxidized NADH/min/well. Finally, cytotoxicity was calculated as the net ratio  
303 between extracellular and total (intracellular + extracellular) LDH activities.

304

### 305 **2.6.3. Human keratinocyte cell viability**

306 Cell viability was evaluated using 3-(4,5-dimethylthiazol-2-yl)-2,5-diphenyltetrazolium bromide  
307 (MTT) assay. HaCaT cells were incubated for 24 h with/without 1 mg/mL Vm, either free or carried by  
308 VmLNBs, in a humidified CO<sub>2</sub>/air-incubator at 37°C. Thereafter, 20  $\mu\text{L}$  of 5 mg/mL MTT in PBS were  
309 added to cells for 3 additional hours at 37 °C. The plates were then centrifuged, the supernatants  
310 discarded and the dark blue formazan crystals dissolved using 100  $\mu\text{L}$  of lysis buffer containing 20 %  
311 (w/v) sodium dodecyl sulfate, 40 % N,N-dimethylformamide (pH 4.7 in 80 % acetic acid). The plates  
312 were then read on Synergy HT microplate reader at a test wavelength of 550 nm and at a reference  
313 wavelength of 650 nm.

314

## 315 **2.7. Microbiological assays**

316

### 317 ***2.7.1. Determination of vancomycin antimicrobial activity against MRSA***

318 Vm solutions were freshly prepared for each experiment. Determination of the minimum inhibitory  
319 concentration (MIC) of vancomycin was carried by the microdilution broth method according to the  
320 latest Clinical and Laboratory Standards Institute (CLSI) guidelines (CLSI 2012). Interpretation of the  
321 results was performed as outlined in the above mentioned CLSI guidelines (CLSI 2012).

322

### 323 ***2.7.2. In vitro antibacterial efficiency of VmLNBs against MRSA.***

324 MRSA, isolated from human ulcerated wounds (Infermi Hospital, Biella, Italy), was cultured over  
325 night at 37°C in TSB. After incubation, bacteria were re-suspended in 100 mL of TSB, harvested by 10

326 min centrifugation at 4,000 rpm, diluted in TSB to  $10^4$  colony-forming-unit (CFU)/mL, as confirmed  
327 by colony counts on TSA, and then incubated in TSB with VmLNBS, loaded with Vm at different  
328 concentrations (1, 0.1, 0.01, and 0.004 mg/mL), in sterile sampling tubes for 2, 3, 4, 6, and 24 hours at  
329 37°C. Controls represented by either bacteria incubated in TSB, bacteria incubated with blank NBs or  
330 bacteria incubated in the presence of free Vm at different concentrations (1, 0.1, 0.01 and 0.004  
331 mg/mL), were also performed. At each incubation time, serial 10-fold dilutions in saline solution (0.9%  
332 NaCl) were prepared from each sample, and 100  $\mu$ L of each dilution were spread on TSA, so that the  
333 number of CFU/mL could be determined.

334

### 335 ***2.7.3. Imaging with confocal laser scanning microscopy***

336 MRSA bacteria were grown in TSB at 37°C in agitation until reaching the concentration of  $1 \times 10^9$   
337 CFU/mL. Then, 1 mL aliquot of bacteria was pelleted (3000g x 10 min at 4°C), resuspended in PBS 1x  
338 and incubated with 6-coumarin-labeled VmLNBS, 6-coumarin-labeled NBs, or FITC-labeled Vm at a  
339 dilution of 1:11, as for previous experiments performed on eukaryotic cells. Each sample was placed on  
340 orbital shaker (160 rpm) in the dark at 37°C for 2h and 4h. After incubation, one drop from each  
341 suspension was streaked on poly-L-lysine-coated microscope slides and allowed to dry. Then, bacteria  
342 were stained with iodide propidium (PI) in PBS 1X and again allowed to dry. Fluorescence images  
343 were taken with an Olympus IX70 inverted laser scanning confocal microscope, and captured using  
344 FluoView 200 software.

345

### 346 ***2.8. Statistical analysis***

347 At least three independent experiments, each one in duplicate or triplicate, were performed for every  
348 investigational study. Numerical data are shown as means  $\pm$  SEM for inferential results or as means  $\pm$   
349 SD for descriptive results (see Cumming et al., 2007 for an exhaustive review). Imaging data are shown



350 as representative pictures. All data were analyzed by a one-way Analysis of Variance (ANOVA)  
351 followed by Tukey's post-hoc test (software: SPSS 16.0 for Windows, SPSS Inc., Chicago, IL).  $P < 0.05$   
352 were considered significant.

353

### 354 **3. Results**

355

#### 356 **3.1. Characterization of VmLNB and control (blank NB and Vm) formulations**

357 Before NB production, the interaction between dextran sulfate and Vm was firstly investigated to  
358 optimize Vm/dextran sulfate ratio. Results indicated that Vm was complexed at 99% by dextran sulfate  
359 solution until the concentration of 0.5 mg/mL (data not shown). The Vm/dextran sulfate ratio was  
360 calculated corresponding to 2:1 (w/w). Based on this preliminary information, NBs were prepared  
361 according to the protocol described in the Materials and Methods section. After manufacturing,  
362 VmLNB and blank NB formulations (with or without 6-coumarin in the inner core) were characterized  
363 physico-chemically. Results are shown in **Figure 2** and **Table 1**. Both VmLNBs and NBs displayed  
364 spherical shapes with a core-shell structure by TEM analyses. All sizes were in the nanometer range,  
365 with all formulations displaying around 300 nm as a value for average diameters. All polydispersity  
366 indexes were included between 0.22 and 0.25. Zeta potentials ranged from -34 mV (NBs) to -29 mV  
367 (VmLNBs). The loading of Vm in the NB structure did not significantly affect the viscosity of the  
368 formulations. NBs were able to load Vm with an encapsulation efficiency of 86% and loading capacity  
369 of 29%.

370

#### 371 **3.2. Stability of VmLNB and control (blank NB and Vm) formulations**

372 NB and VmLNB formulations proved to be physically stable over time, as confirmed by long-term  
373 checking of the parameters assessed in the previous paragraph. Indeed, the obtained values did not  
374 remarkably change up to six months after the manufacturing of the formulations stored at 4 °C (data  
375 not shown). Furthermore, the chemical stability of the drug was comparatively checked between free  
376 Vm solution and VmLNB aqueous suspension either over time (up to 14 days) or at different  
377 temperatures (25°C and 37°C). As shown in **Figure 3**, the drug resulted much more stable from a

378 chemical point of view when properly incorporated in the nanocarrier (VmLNBS) than as such in  
379 solution.

380

### 381 **3.3. Human biocompatibility**

382

383 The potential toxicity of Vm solution and VmLNB suspension on human skin cells was assessed by  
384 testing *in vitro* cultured HaCaT keratinocytes. Cells were incubated for 24 h alone, with 10% v/v Vm  
385 solution, or with VmLNB nanosuspensions in normoxic conditions (20% O<sub>2</sub>). Thereafter, cytotoxicity  
386 was analyzed by LDH assay, and cell viability by MTT assay. As shown in **Figure 4**, neither Vm nor  
387 VmLNBS did show significant toxic effects and HaCaT cell viability was not significantly affected by  
388 either formulation.

389

### 390 **3.4. *In vitro* drug release from VmLNBS**

391 *In vitro* drug release from VmLNB nanosuspension and free Vm solution were comparatively  
392 evaluated over time. As shown in **Figure 5** (time course studies up to 6 h) and **Table 2** (end-point data  
393 up to 24 h), 1 mg/mL Vm release from VmLNBS was slow and prolonged over time, compared to free  
394 drug solution diffusion. No initial burst effect was observed indicating Vm incorporation in NB shell.  
395 Further information on additional incubation times and drug concentrations for VmLNBS is available in  
396 Supplementary Materials (**Table S3**). Vm/VmLNB drug release ratios at different times (2, 3, 4, 6, and  
397 24 h) were also calculated (see **Table 2**), in order to allow normalization of the results from treatment  
398 with VmLNBS in the microbiological experiments described in the following paragraph.

399

400

401

### 402 **3.5. *In vitro* antimicrobial activity of VmLNBS**

403 According to preliminary microbiological analyses performed on the MRSA strain employed in the  
404 present experiments, 0.004 mg/mL resulted as the MIC value for Vm. Therefore, decreasing Vm  
405 concentrations from 1 mg/mL (used for the studies described in the previous paragraphs) to 0.004  
406 mg/mL (MIC value) were employed in a series of experiments aimed at comparatively evaluating Vm  
407 (either free or carried by VmLNBS) antibacterial effectiveness against MRSA. Bacteria were incubated  
408 at different times (2, 3, 4, 6, and 24 h) either alone (ctr) or with free Vm, VmLNBS, or blank NBs. The  
409 initial drug concentrations (1; 0.1; 0.01; and 0.004 mg/mL) loaded on VmLNBS were the same as those  
410 solved in free Vm solution. However, as emerged in the previous paragraph, drug release from  
411 VmLNBS is significantly slower than free Vm solution diffusion. For this reason, before proceeding  
412 with the analysis of the results, all values on bacterial growth referring to Vm- and VmLNB-treated  
413 samples were normalized upon time-dependent Vm/VmLNB drug release ratios shown in **Table 2**.  
414 Normalized results are shown in **Figure 6**, whereas raw data are available in Supplementary Materials  
415 (**Figure S2**). 1 mg/mL Vm effectively inhibited bacterial growth at all times, independently from being  
416 free or carried by the nanocarrier. Lower drug concentrations of free Vm solution were effective  
417 against MRSA only after longer times of incubation (at least 3 h for 0.1 mg/mL and 0.01 mg/mL Vm;  
418 and at least 4 h for 0.004 mg/mL Vm). Interestingly, Vm antibacterial efficacy was significantly  
419 improved when the drug was carried by VmLNBS. Indeed, VmLNB-dependent inhibition of bacterial  
420 growth was significantly enhanced compared to free Vm solution, at all drug concentrations.  
421 Additionally, compared to free Vm solution, VmLNB antibacterial effects appeared earlier, as they  
422 were already evident after 2 h of incubation (the first time-point of the observational period) at all Vm  
423 concentrations. Blank NBs did not show any antibacterial activity.

424 Further analysis by confocal microscopy (**Figure 7**) displayed that MRSA avidly internalized free  
425 fluorescent Vm already after 2 h of incubation, but not fluorescent VmLNBS. Fluorescent Vm-free NBs  
426 did adhere to the bacterial cell wall without being internalized.

### 427 **3.6. US-triggered drug permeation**

428 The ability of US to promote Vm permeation through the skin was assayed by employing a purposely  
429 modified Franz cell constituted by a donor and a recipient chamber separated by a pig skin layer (see  
430 **Figure 8A** for a schematic representation of the apparatus). As shown in **Figure 8B**, the administration  
431 of US ( $t = 10$  min;  $f = 2.5$  MHz;  $P = 5$  W) strongly induced VmLNBS to deliver the antibiotic drug  
432 from the donor chamber throughout the pig skin membrane into the recipient chamber up to 6 h.  
433 Furthermore, drug accumulated in the skin after US treatment reached  $158 \mu\text{g}/\text{cm}^2$  after 6 hours.

434

435

436

437

#### 438 **4. Discussion**

439

440 Vm currently represents the main stay against MRSA infections (Koyama et al., 2013; Kullar et al.,  
441 2016). However, Vm administration raises several issues that urgently need to be faced, including its  
442 marked instability, low oral bioavailability, complex concentration-time profile, low tissue penetration  
443 (ranging from 10% in diabetic to 30% in normal skin and soft tissues), and several adverse effects  
444 (Mawhinney et al., 1992; Raverdy et al., 2013; Vandecasteele et al., 2012; Vidal et al., 1992; Giandalia  
445 et al., 2001). In the attempt to counteract these drawbacks, thus improving the effectiveness of Vm  
446 delivery, some novel nanocarriers have been developed: i) Vm coupling to chitosan as an ocular drug  
447 delivery vehicle for topical use in rabbit eyes has appeared more effective than carrier-free Vm  
448 (Khangtragool et al., 2011); ii) PEGylated liposomal Vm enhanced the effective treatment of MRSA  
449 pneumonia and simultaneously reduced the nephrotoxicity risk compared with conventional and non-  
450 PEGylated Vm formulations (Muppidi et al., 2011); iii) Vm-loaded liposomes, stabilized with chitosan  
451 modified gold nanoparticles bounded to their surface, have proven effective in inhibiting the bacterial  
452 growth (Pornpattananangkul et al., 2011); and iv) Vm-containing trehalose and hydroxyethylcellulose  
453 spherical matrices have been developed as new delivery systems suitable for topical applications on  
454 extensive and purulent wounds (Giandalia et al., 2001). Recently, Vm-loaded polymersomes were  
455 developed from a novel pegylated oleic acid polymer for sustained antibiotic delivery (Omolo et al.,  
456 2017). Overall, these works represent the proof-of-principle for the feasibility of choice of nanocarriers,  
457 as alternative drug delivery systems to obtain the desired drug release rates and bioavailability  
458 (Kalhapure et al., 2015). However, the effectiveness of those nanocarriers was seriously undermined by  
459 their poor ability to cross the *stratum corneum*, a skin barrier displaying low permeability unless proper  
460 exogenous physical stimuli are provided (Azagury et al., 2014; Park et al, 2012).

461 For these reasons, the present study aimed at developing Vm nanocarriers as a new platform to be  
462 effectively and safely employed for Vm topical administration to treat wound infections. To this  
463 purpose, NBs with core-shell nanostructures were identified as first choice carriers due to their known  
464 benefits in association with drug delivery, including small size, stability, suitability for drug loading,  
465 responsiveness to external stimuli such as US, and controlled drug release abilities (Marano et al.,  
466 2016; Cavalli et al., 2009a; Cavalli et al., 2009b; Cavalli et al., 2016). In this study, dextran sulfate was  
467 chosen as main constituent of the polysaccharidic shell as a consequence of the large amount of data  
468 from the literature supporting dextran biocompatibility (Bos et al., 2005; De Groot et al., 2001).  
469 Encouragingly, dextran-based hydrogels have already been employed as matrices in tissue engineering,  
470 without showing signs of inflammation *in vivo* (Möller et al., 2007), and recent toxicological studies  
471 have shown that dextran, as well as the products from its mechano-chemical processing, can be  
472 classified as class 4 (low-toxicity) substances (Dushkin et al., 2013). Moreover, dextran sulfate presents  
473 a negative charge that can electrostatically interact with the positive charged Vm. On the other hand,  
474 PFP was employed as principal constituent of the inner core, since it is the most widely used  
475 fluorocarbon in oxygenating emulsions and NB formulations (Cabralles and Intaglietta, 2013, Castro  
476 and Briceno, 2010). In order to load Vm, dextran sulfate-shelled/PFP-cored NBs were then  
477 functionalized by exploiting the electrostatic interactions occurring between the negatively charged  
478 sulfate groups of the shell and the protonated amino groups of the drug. The obtained VmLNBS  
479 displayed a spherical shape and a well-defined core-shell structure with a polymeric shell thickness of  
480 about 40 nm, average diameters of 300 nm, viscosity of 1.25 cP, and negatively charged surfaces. Of  
481 note, the observed decrease of zeta potential values of ~ 15 % for VmLNBS (around -29 mV) with  
482 respect to blank NBs (around -34 mV) confirmed the occurrence of electrostatic interactions between  
483 positive amino groups of the drug and negative sulfate groups of the polymer, leading to a partial

484 charge neutralization of the bubble surface and allowing a good Vm encapsulation efficiency (86%)  
485 and loading capacity (29%) in the NB systems.

486 In addition, it should be noticed that since the zeta potential measures charge repulsion or attraction  
487 between particles, it represents a fundamental parameter to avoid nanoparticle aggregation, with zeta  
488 potentials lower than -25 mV or larger than +25 mV being generally required for physical stability of  
489 colloid systems (Shah and Eldridge, 2014). The stability of VmLNB formulations was further  
490 confirmed by long-term checking of their size, surface charge, and viscosity values, which did not  
491 show any significant changes up to six months after manufacturing, stored at 4 °C. On the other hand,  
492 drug stability was comparatively checked between free Vm solution and VmLNB suspension either  
493 over time (up to 14 days) or at different temperatures (25°C and 37°C), revealing an increased stability  
494 for Vm when properly encapsulated in the nanocarriers. This appears as an undoubtedly advantageous  
495 feature for VmLNB formulations, since they might prove useful to overcome the reported instability of  
496 Vm in aqueous solutions at body temperature (Mawhinney et al., 1992, Raverdy et al., 2013).

497 Interestingly, VmLNBs displayed a slow and prolonged drug release kinetics compared to Vm aqueous  
498 solution, with only 16% of the drug being released from VmLNBs after 6 h. These data support the  
499 hypothesis that VmLNBs may be employed as an effective drug reservoir until reaching the target site,  
500 where the antibiotic would be released upon sonication at an appropriate moment only. The features of  
501 VmLNBs might be exploited for the design of innovative wound dressing following their inclusion in  
502 polymeric base. Indeed, NBs can be dispersed in polymer gel without changing physico-chemical  
503 characteristics, as previously showed (Prato et al., 2015). Another intriguing feature of VmLNBs relies  
504 on the reported evidence that surface charges play a pivotal role in making a nanoparticle suitable for  
505 topical treatment, since they enhance its interaction with the skin and improve its therapeutic effect on  
506 inflamed cutaneous tissues, either without (Abdel-Mottaleb et al., 2012) or with concomitant US  
507 treatment (Lopez et al., 2011). Although cationic nanoparticles are generally preferred for topical



508 treatment due to the anionic nature of the skin (Wu et al., 2010), some authors have shown that anionic  
509 nanoparticles can be more effective (Lee et al., 2013) and less toxic (Ryman-Rasmussen et al., 2007)  
510 than the cationic ones. These latter data appear consistent with our results through investigation by  
511 biochemical assays to assess VmLNB biocompatibility with human skin tissues. Indeed, VmLNBs did  
512 not induce any *in vitro* cytotoxic effects on HaCaT keratinocytes, a skin cell line that was originally  
513 immortalized from a 62-year old donor (Boukamp et al., 1988). This peculiar information strengthens  
514 remarkably the evidence on VmLNB safety for future topical applications.

515 VmLNB and carrier-free Vm antimicrobial activity against MRSA were comparatively investigated,  
516 also analyzing Vm and NB physical interaction with the bacterial cell wall by confocal microscopy.  
517 Interestingly, VmLNBs were more effective in MRSA bacterial growth inhibition than free Vm,  
518 promoting enhanced and earlier antibacterial effects, although they were not internalized by bacteria,  
519 opposite to free Vm. This behavior appears to be a likely consequence of time-sustained release of Vm  
520 from VmLNBs.

521 Notably, an important issue that requires caution while evaluating the feasibility for any topical drug  
522 treatment is represented by the considerably low degree of permeability of the skin, the primary  
523 defense system for the body. This organ consists of several layers, including the *stratum corneum*, the  
524 epidermis, and the dermis. In particular the *stratum corneum* - composed of corneocytes interspersed in  
525 a laminate of compressed keratin and intercorneocyte lipid lamellae - is very poorly permeable to  
526 foreign molecules and represents the main obstacle to transdermal drug delivery (Naik et al., 2000).  
527 However, an ideal antibiotic drug formulation should be efficiently localized in the epidermis/dermis  
528 and provide a sustained drug release over time (Prabhu et al., 2012). To allow a drug to penetrate the  
529 skin, several approaches have been proposed, including skin patches, iontophoresis, chemical  
530 enhancers, and US-triggered sonophoresis (Park et al., 2014).

531 Interestingly, antimicrobial properties have been reported for US, although its effectiveness strongly  
532 varies depending on the targeted type of pathogen (fungi vs bacteria; cocci vs bacilli; Gram-positive vs  
533 Gram-negative) (Sango et al., 2014). Furthermore, synergistic effects between US and antibiotics have  
534 been reported in a series of studies: i) antibiotic treatment coupled with US irradiation resulted in  
535 enhanced bactericidal activity against both Gram-positive and Gram-negative bacteria, especially for  
536 aminoglycosides (Yu et al., 2012); ii) the combination of Vm and US decreased *S. aureus* viable counts  
537 by two orders of magnitude compared to Vm alone (Ayan et al., 2008); and iii) the addition of NB-  
538 enhanced US to doxycycline treatment improved the drug effectiveness in eradicating intracellular  
539 *Chlamydia trachomatis* (Ikeka-Dantsuji et al., 2011). US-dependent enhancement of antibiotic action  
540 on biofilms was named as a ‘bioacoustic effect’. Interestingly, Vm transfer through *S. epidermidis*  
541 biofilms was shown to be significantly enhanced by US, with bubbles being able to increase the biofilm  
542 permeability to Vm (Dong et al., 2013).

543 As discussed previously, VmLNBS can be effectively employed as an important reservoir to store the  
544 drug until trespassing the *stratum corneum* of the skin and reaching the target site. In order to achieve  
545 the latter goal, US was assayed for its ability to induce VmLNBS to trespass an *in vitro* cutaneous layer,  
546 thereby releasing Vm throughout the skin. Notably, the skin from the pig ear is widely recognized as a  
547 good model for human skin permeability, since it displays human-like histological and physiological  
548 properties, including epidermal thickness and composition, dermal structure, lipid content and general  
549 morphology (Dick and Scott, 1992). The validity of the porcine model has been established by  
550 comparing the permeability of simple marker molecules with the corresponding values across human  
551 skin (Herkenne et al., 2006, Sekkat et al., 2002). Therefore, the porcine ear skin represents so far the  
552 most accountable *in vitro* model to mimic the human skin in studies on percutaneous penetration  
553 (Jacobi et al., 2007). In our experiments, US appeared essential to promote Vm release from VmLNBS  
554 throughout the pig skin layers, in line with previous reports on NBs and sonophoresis. On the contrary,

555 the passive transport of free vancomycin hydrochloride was negligible, being a charged and hydrophilic  
556 molecule. The amount of Vm accumulated in the skin after US application combined with NBs was  
557 greater than MIC value.

558

## 559 **5. Conclusions**

560 In the present work, dextran sulfate-shelled and PFP-filled NBs were developed for Vm delivery.  
561 VLNBs proved to be effective in MRSA bacterial killing without showing toxic effects on human  
562 keratinocytes. The combination of NBs and US enhanced Vm permeation through pig skin and  
563 promoted drug skin accumulation. Based on these results, Vm topical administration through proper  
564 NB formulations might be a promising strategy for the local treatment of MRSA skin infections. The  
565 study represents the proof of concept for the future development of advanced multifunctional  
566 therapeutic systems to treat infected wounds.

567 **Acknowledgements**

568 The present work was supported by funds from University of Torino (ex 60% to RC and RS),  
569 Compagnia di San Paolo (ORTO11CE8R 2011 to CG and Torino\_call2014\_L2\_207 to AMC), and  
570 Fondazione Cariplo (HyWonNa project grant to MP). Thanks are due to Aurelio Malabaila for  
571 providing MRSA strain and to Giorgio Gribaudo for allowing to use his lab facilities to perform  
572 confocal microscopy studies.

573

574

575

576

577 **References**

578

579 Abdel-Mottaleb, M.M., Moulari, B., Beduneau, A., Pellequer, Y., Lamprecht, A., 2012. Surface-  
580 charge-dependent nanoparticles accumulation in inflamed skin. *J. Pharm. Sci.*101, 4231-4239.

581

582 Ayan, İ., Aslan, G., Çömelekoğlu, Ü., Yılmaz, N., Çolak, M., 2008. The effect of low-intensity pulsed  
583 sound waves delivered by the Exogen device on *Staphylococcus aureus* morphology and genetics. *Acta*  
584 *orthop. traumatol. turc.* 42(4), 272-277.

585

586 Azagury, A., Khoury, L., Enden, G., Kost, J., 2014. Ultrasound mediated transdermal drug  
587 delivery. *Adv. drug del. rev.* 72, 127-143.

588

589 Banche, G., Prato, M., Magnetto, C., Allizond, V., Giribaldi, G., Argenziano, M., Khadjavi, A., Gulino,  
590 G.R., Finesso, N., Mandras, N., Tullio, V., Cavalli, R., Guiot, C., Cuffini, A.M., 2015. Antimicrobial  
591 chitosan nanodroplets: new insights for ultrasound-mediated adjuvant treatment of skin infection.  
592 *Future Microbiol.* 10(6), 929-939. doi: 10.2217/fmb.15.27. PubMed PMID: 26059617.

593

594 Basilico, N., Magnetto, C., D'Alessandro, S., Panariti, A., Rivolta, I., Genova, T., Khadjavi, A., Gulino,  
595 G.R., Argenziano, M., Soster, M., Cavalli, R., Giribaldi, G., Guiot, C., Prato, M., 2015. Dextran-  
596 shelled oxygen-loaded nanodroplets reestablish a normoxia-like pro-angiogenic phenotype and  
597 behavior in hypoxic human dermal microvascular endothelium. *Toxicol. Appl. Pharmacol.* 288(3), 330-  
598 338. doi: 10.1016/j.taap.2015.08.005. Epub 2015 Aug 12. PubMed PMID: 26276311.

599

600 Bos, G.W., Hennink, W.E., Brouwer, L.A., den Otter, W., Veldhuis, F.J., van Nostrum, C.F., van Luyn  
601 M.J., 2005. Tissue reactions of in situ formed dextran hydrogels crosslinked by stereocomplex  
602 formation after subcutaneous implantation in rats. *Biomaterials* 26, 3901–3909.

603

604 Boukamp, P., Dzarlieva-Petrusevska, R.T., Breitkreuz, D., Hornung, J., Markham, A., Fusenig, N.E.,  
605 1988. Normal keratinization in a spontaneously immortalized aneuploid human keratinocyte cell line. *J.*  
606 *Cell. Biol.* 106, 761-771.

607

608 Cabrales, P., Intaglietta, M., 2013. Blood substitutes: evolution from noncarrying to oxygen- and gas-  
609 carrying fluids. *ASAIO J.* 59, 337-354.

610

611 Castro, C.I., Briceno, J.C., 2010. Perfluorocarbon-based oxygen carriers: review of products and trials.  
612 *Artif. Organs.* 34, 622-634.

613

614 Cavalli, R., Bisazza, A., Rolfo, A., Balbis, S., Madonnaripa, D., Caniggia, I., Guiot, C., 2009a.  
615 Ultrasound-mediated oxygen delivery from chitosan nanobubbles. *Int. J. Pharm.* 378, 215–217.

616

617 Cavalli, R., Bisazza, A., Giustetto, P., Civra, A., Lembo, D., Trotta, G., Guiot, C., Trotta, M., 2009b.  
618 Preparation and characterization of dextran nanobubbles for oxygen delivery. *Int. J. Pharm.* 381, 160-  
619 165.

620

621 Cavalli, R., Bisazza, A., Trotta, M., Argenziano, M., Civra, A., Donalisio, M., Lembo, D., 2012. New  
622 chitosan nanobubbles for ultrasound-mediated gene delivery: preparation and in vitro characterization.  
623 *Int. J. Nanomed.* 7, 3309-3318.

624 Cavalli, R., Bisazza, A., Lembo, D., 2013. Micro-and nanobubbles: A versatile non-viral platform for  
625 gene delivery. *Int. J. Pharm.* 456(2), 437-445.

626

627 Cavalli, R., Soster, M., Argenziano, M., 2016. Nanobubbles: a promising efficient tool for therapeutic  
628 delivery. *Ther. Deliv.* 7(2), 117-138. doi: 10.4155/tde.15.92. Epub 2016 Jan 15. PubMed PMID:  
629 26769397.

630

631 Clinical and Laboratory Standards Institute. Performance standards for antimicrobial susceptibility  
632 testing. Twenty-second informational supplement. Document M100-S22. Vol . 32, No. 3. Wayne, PA:  
633 CLSI; 2012.

634

635 Cumming, G., Fidler, F., Vaux, D.L., 2007. Error bars in experimental biology. *J Cell Biol.* 177, 7-11.

636

637 Daeschlein, G., 2013. Antimicrobial and antiseptic strategies in wound management. *Int. Wound J.*  
638 10(1), 9-14. doi: 10.1111/iwj.12175. Review. PubMed PMID:24251838.

639

640 De Groot C.J., Van Luyn, M.J.A., Van Dijk-Wolthuis, Cadée, J.A., Plantinga, J.A., Den Otter, W.,  
641 Hennink, W.E., 2001. In vitro biocompatibility of biodegradable dextran-based hydrogels tested with  
642 human fibroblast. *Biomaterials* 22, 1197–1203.

643

644 Delalande, A., Postema, M., Mignet, N., Midoux, P., Pichon, C., 2012. Ultrasound and microbubble-  
645 assisted gene delivery: recent advances and ongoing challenges. *Ther. Deliv.* 3, 1199-1215.

646

647 Dick, I.P., Scott, R.C. 1992. Pig ear skin as an in-vitro model for human skin permeability. *J. Pharm.*  
648 *Pharmacol.* 44, 640–645.

649

650 Diehr, P., O'Meara, E.S., Fitzpatrick, A., Newman, A.B., Kuller, L., Burke, G., 2008. Weight,  
651 mortality, years of healthy life, and active life expectancy in older adults. *J. Am. Geriatr. Soc.* 56(1),  
652 76-83. Epub 2007 Nov 20. PubMed PMID: 18031486; PubMed Central PMCID: PMC3865852.

653

654 Dong, Y., Chen, S., Wang, Z., Peng, N., Yu, J., 2013. Synergy of ultrasound microbubbles and  
655 vancomycin against *Staphylococcus epidermidis* biofilm. *J. Antimicrob. Chemother.* 68, 816-826.

656

657 Dushkin, A.V., Meteleva, E.S., Tolstikova, T.G., Pavlova, A.V., Khvostov, M.V. 2013. Gel  
658 chromatographic and toxicological studies of the mechanochemical transformations of water-soluble  
659 polysaccharides. *Pharm. Chem. J.* 46, 630-633.

660

661 Fokong, S., Theek, B., Wu, Z., Koczera, P., Appold, L., Jorge, S., Resch-Genger, U., VanZandvoort,  
662 M., Storm, G., Kiessling, F., Lammers, T., 2012. Image-guided, targeted and triggered drug delivery to  
663 tumors using polymer-based microbubbles. *J. Control. Rel.* 163, 75–81.

664

665 Giandalia, G., De Caro, V., Cordone, L., Giannola, L.I. 2001. Trehalose-hydroxyethylcellulose  
666 microspheres containing vancomycin for topical drug delivery. *Eur. J. Pharm. and Biopharm.: official*  
667 *journal of Arbeitsgemeinschaft fur Pharmazeutische Verfahrenstechnik e.V.* 52, 83-89.

668



669 Guiot, C., Pastore, G., Napoleone, M., Gabriele, P., Trotta, M., Cavalli, R., 2006. Thermal response of  
670 contrast agent microbubbles: preliminary results from physico-chemical and US-imaging  
671 characterization. *Ultrasonics*. 44(1), 127-130. Epub 2006 Jun 30. PubMed PMID: 17056082.

672

673 Gulino, G.R., Magnetto, C., Khadjavi, A., Panariti, A., Rivolta, I., Soster, M., Argenziano, M., Cavalli,  
674 R., Giribaldi, G., Guiot, C., Prato, M., 2015. Oxygen-Loaded Nanodroplets Effectively Abrogate  
675 Hypoxia Dysregulating Effects on Secretion of MMP-9 and TIMP-1 by Human Monocytes. *Mediators  
676 Inflamm.* 2015, 964838. doi: 10.1155/2015/964838. Epub 2015 Mar 23. PubMed PMID: 25878404;  
677 PubMed Central PMCID: PMC4386605.

678

679 Gurusamy, K.S., Koti, R., Toon, C.D., Wilson, P., Davidson, B.R., 2013. Antibiotic therapy for the  
680 treatment of methicillin-resistant *Staphylococcus aureus* (MRSA) infections in surgical wounds.  
681 *Cochrane Database Syst. Rev.* 20, 8:CD009726. doi: 10.1002/14651858.CD009726.pub2. Review.  
682 PubMed PMID: 23963687.

683

684 Herkenne, C., Naik, A., Kalia, Y.N., Hadgraft, J., Guy, R.H., 2006. Pig ear skin ex vivo as a  
685 model for in vivo dermatopharmacokinetic studies in man. *Pharm. Res.* 23, 1850-1856.

686

687 Ikeda-Dantsuji, Y., Feril, L. B., Tachibana, K., Ogawa, K., Endo, H., Harada, Y., Suzuki, R.,  
688 Maruyama, K., 2011. Synergistic effect of ultrasound and antibiotics against *Chlamydia trachomatis*-  
689 infected human epithelial cells in vitro. *Ultrason. sonochem.* 18(1), 425-430.

690

691 Jacobi, U., Kaiser, M., Toll, R., Mangelsdorf, S., Audring, H., Otberg, N., Sterry, W., Lademann, J.,  
692 2007. Porcine ear skin: an in vitro model for human skin. *Skin Research and Technology* 13(1), 19-24.

693 Karshafian, R., Bevan, P.D., Williams, R., Samac, S., Burns, P.N., 2009. Sonoporation by ultrasound-  
694 activated microbubble contrast agents: effect of acoustic exposure parameters on cell membrane  
695 permeability and cell viability. *Ultrasound Med. Biol.* 35, 847-860.

696

697 Khadjavi, A., Magnetto, C., Panariti, A., Argenziano, M., Gulino, G.R., Rivolta, I., Cavalli, R.,  
698 Giribaldi, G., Guiot, C., Prato, M., 2015. Chitosan-shelled oxygen-loaded nanodroplets abrogate  
699 hypoxia dysregulation of human keratinocyte gelatinases and inhibitors: New insights for chronic  
700 wound healing. *Toxicol. Appl. Pharmacol.* 286(3), 198-206. doi: 10.1016/j.taap.2015.04.015. Epub  
701 2015 Apr 30. PubMed PMID: 25937238.

702

703 Kalhapure, R.S., Suleman, N., Mocktar, C., Seedat, N., Govender, T., 2015. Nanoengineered Drug  
704 Delivery Systems for Enhancing Antibiotic Therapy. *J. Pharm. Sci.* 104, 872–905.

705

706 Khangtragool, A., Ausayakhun, S., Leesawat, P., Laokul, C., Molloy, R., 2011. Chitosan as an ocular  
707 drug delivery vehicle for vancomycin. *J. App. Pol. Sci.* 122, 3160-3167.

708

709 Koyama, N., Inokoshi, J., Tomoda, H., 2012. Anti-infectious agents against MRSA. *Molecules* 18(1),  
710 204-224. doi: 10.3390/molecules18010204.

711

712 Kullar, R., Sakoulas, G., Deresinski, S., van Hal, S. J., 2016. When sepsis persists: a review of MRSA  
713 bacteraemia salvage therapy. *J. Antimicrob. Chemother.* 71, 576-586.

714

715 Lazarus, G.S., Cooper, D.M., Knighton, D.R., Percoraro, R.E., Rodeheaver, G., Robson, M.C., 1994.  
716 Definitions and guidelines for assessment of wounds and evaluation of healing. *Wound Repair Regen.*  
717 2(3), 165-170. PubMed PMID: 17156107.

718

719 Lee, O., Jeong, S.H., Shin, W.U., Lee, G., Oh, C., Son, S.W., 2013. Influence of surface charge of gold  
720 nanorods on skin penetration. *Skin Res. Technol.* 19, e390-e396.

721

722 Lopez, R.F., Seto, J.E., Blankschtein, D., Langer, R., 2011. Enhancing the transdermal delivery of rigid  
723 nanoparticles using the simultaneous application of ultrasound and sodium lauryl sulfate. *Biomaterials.*  
724 32, 933-941.

725

726 Magnetto, C., Prato, M., Khadjavi, A., Giribaldi, G., Fenoglio, I., Jose, J., Gulino, G.R., Cavallo, F.,  
727 Quaglino, E., Benintende, E., Varetto, G., Troia, A., Cavalli, R., Guiot, C., 2014. Ultrasound-activated  
728 decafluoropentane-cored and chitosan-shelled nanodroplets for oxygen delivery to hypoxic cutaneous  
729 tissues. *RSC Advances* 4, 38433-38441.

730

731 Marano, F., Argenziano, M., Frairia, R., Adamini, A., Bosco, O., Rinella, L., Fortunati, N., Cavalli, R.,  
732 Catalano, M.G., 2016. Doxorubicin-Loaded Nanobubbles Combined with Extracorporeal Shock  
733 Waves: Basis for a New Drug Delivery Tool in Anaplastic Thyroid Cancer. *Thyroid* 26(5), 705-716

734

735 Markova, A., Mostow, E.N., 2012. US skin disease assessment: ulcer and wound care. *Dermatol. Clin.*  
736 30(1), 107-111. ix. doi: 10.1016/j.det.2011.08.005. Review. PubMed PMID: 22117872.

737

738 Marxer, E.E.J., Brüßler, J., Becker, A., Schümmelfeder, J., Schubert, R., Nimsy, C., Bakowsky, U.,  
739 2011. Development and characterization of new nanoscaled ultrasound active lipid dispersions as  
740 contrast agents. *Eur. J. Pharm. Biopharm.* 77, 430–437.

741

742 Mawhinney, W.M., Adair, C.G., Gorman, S.P., McClurg, B., 1992. Stability of vancomycin  
743 hydrochloride in peritoneal dialysis solution. *Am. J. Hosp. Pharm.* 49(1), 137-139. PubMed PMID:  
744 1570857.

745

746 Möller, S., Weisser, J., Bischoff, S., Schnabelrauch, M., 2007. Dextran and hyaluronan methacrilate  
747 based hydrogels as matrices for soft tissue reconstruction. *Biomol. Eng.* 24, 496–504.

748

749 Muppidi, K., Wang, J., Betageri, G., Pumerantz, A.S. 2011. PEGylated liposome encapsulation  
750 increases the lung tissue concentration of vancomycin. *Antimicrob. Agents Chemother.* 55(10), 4537-  
751 4542.

752

753 Naik, A., Kalia, Y.N., Guy, R.H., 2000. Transdermal drug delivery: overcoming the skin's barrier  
754 function. *Pharm. Sci. Technol. Today.* 3, 318–326.

755

756 Omolo, C.A., Kalhapure, R.S., Jadhav, M., Rambharose, S., Mocktar, C., Ndesendo, V.M., Govender,  
757 T. 2017. PEGylated oleic acid: A promising amphiphilic polymer for nano-antibiotic delivery. *Eur. J.*  
758 *Pharm. Biopharm.* 112, 96-108.

759

760 Park, D., Ryu, H., Kim, H.S., Kim, Y.S., Choi, K.S., Park, H., Seo J., 2012. Sonophoresis Using  
761 Ultrasound Contrast Agents for Transdermal Drug Delivery: An In Vivo Experimental Study.  
762 *Ultrasound Med. & Biol.* 38(4), 642-650.

763

764 Park, D., Park, H., Seo, J., Lee, S., 2014. Sonophoresis in transdermal drug delivery. *Ultrasonics*. 54,  
765 56-65.

766

767 Payne, W.G., Naidu, D.K., Wheeler, C.K., Barkoe, D., Mentis, M., Salas, R.E., Smith, D.J., Robson,  
768 M.C., 2008. Wound healing in patients with cancer. *Eplasty*. 8, e9. PubMed PMID: 18264518; PubMed  
769 Central PMCID: PMC2206003.

770

771 Pornpattananankul, D., Zhang, L., Olson, S., Aryal, S., Obonyo, M., Vecchio, K., Huang, C.M.,  
772 Zhang, L., 2011. Bacterial toxin-triggered drug release from gold nanoparticle-stabilized liposomes for  
773 the treatment of bacterial infection. *J. American Chem. Soc.*133(11), 4132-4139.

774

775 Prabhu, P., Patravale, V., Joshi, M., 2012. Nanocarriers for effective topical delivery of anti-infectives.  
776 *Current Nanoscience* 8, 491-503.

777

778 Prato, M., Magnetto, C., Jose, J., Khadjavi, A., Cavallo, F., Quaglino, E., Panariti, A., Rivolta, I.,  
779 Benintende, E., Varetto, G., Argenziano, M., Troia, A., Cavalli, R., Guiot C., 2015. 2H,3H-  
780 decafluoropentane-based nanodroplets: new perspectives for oxygen delivery to hypoxic cutaneous  
781 tissues. *Plos One* 10(3), e0119769. doi:10.1371/journal.pone.0119769

782

783 Prato, M., Khadjavi, A., Magnetto, C., Gulino, G.R., Rolfo, A., Todros, T., Cavalli, R., Guiot, C., 2016.  
784 Effects of oxygen tension and dextran-shelled/2H,3H-decafluoropentane-cored oxygen-loaded  
785 nanodroplets on secretion of gelatinases and their inhibitors in term human placenta. *Biosci Biotechnol*  
786 *Biochem.* 80(3), 466-472. doi: 10.1080/09168451.2015.1095068. Epub 2015 Nov 2. PubMed PMID:  
787 26523859.

788

789 Price, M., 2010. Community-acquired methicillin-resistant *Staphylococcus aureus*: an ongoing  
790 challenge for WOC nursing. *J Wound Ostomy Continence Nurs.* 37(6), 633-638. doi:  
791 10.1097/WON.0b013e3181feb001. Review. PubMed PMID: 21076263.

792

793 Raverdy V., Ampe, E., Hecq, J.D., Tulkens, P. M., 2013. Stability and compatibility of vancomycin for  
794 administration by continuous infusion. *J. Antimicrob. Chemother.* 68, 1179-1182.

795

796 Ryman-Rasmussen, J.P., Riviere, J.E., Monteiro-Riviere, N.A., 2007. Surface coatings determine  
797 cytotoxicity and irritation potential of quantum dot nanoparticles in epidermal keratinocytes. *J Invest*  
798 *Dermatol.* 127, 143-153.

799

800 Sango, D.M., Abela, D., McElhatton, A., Valdramidis, V.P., 2014. Assisted ultrasound applications for  
801 the production of safe foods. *J. Appl. Microbiol.* 116, 1067-1083.

802

803 Sekkat, N., Kalia, Y.N., Guy, R.H., 2002. Biophysical study of porcine ear skin in vitro and its  
804 comparison to human skin in vivo. *J. Pharm. Sci.* 91, 2376-2381.

805 Shah, R., Eldridge, R., 2014. Optimisation and Stability Assessment of Solid Lipid Nanoparticles using  
806 Particle Size and Zeta Potential. *J. Phys. Sci,* 25, 59–75

807 Sharma, A., Arya, D.K., Dua, M., Chhatwal, G.S., Johri, A.K., 2012. Nano-technology for targeted  
808 drug delivery to combat antibiotic resistance. *Expert Opinion Drug Del.* 9, 1325-1332.

809

810 Vandecasteele, S.J., De Vriese, A.S., Tacconelli, E., 2012. The pharmacokinetics and  
811 pharmacodynamics of vancomycin in clinical practice: evidence and uncertainties. *J. Antim. Chem.* 68,  
812 743-748.

813

814 Vidal, C., González Quintela, A., Fuente, R., 1992. Toxic epidermal necrolysis due to vancomycin.  
815 *Ann Allergy.* 68(4), 345-347. PubMed PMID: 1558331.

816

817 Wu, X., Landfester, K., Musyanovych, A., Guy, R.H., 2010. Disposition of charged nanoparticles after  
818 their topical application to the skin. *Skin Pharmacol Physiol.* 23, 117-123.

819

820 Yin, T., Wang, P., Li, J., Wang, Y., Zheng, B., Zheng, R., Cheng, D., Shuai, X., 2014. Tumor-  
821 penetrating codelivery of siRNA and paclitaxel with ultrasound-responsive nanobubbles hetero-  
822 assembled from polymeric micelles and liposomes. *Biomaterials* 35(22), 5932-5943.

823

824 Yu, H., Chen, S., Cao, P., 2012. Synergistic bactericidal effects and mechanisms of low intensity  
825 ultrasound and antibiotics against bacteria: a review. *Ultrasonics sonochemistry* 19(3), 377-382.

826

827 Zilberman, M., Elsner, J.J., 2008. Antibiotic-eluting medical devices for various applications. *J Control*  
828 *Release* 130(3), 202-215. doi: 10.1016/j.jconrel.2008.05.020. Epub 2008 Aug 6. Review. PubMed  
829 PMID: 18687500.

830 **Figure legends**

831

832 **Figure 1. Schematic structure of VmLNB formulations.** Vm nanocarriers described in the present  
833 work display a core-shell structure. PFP was employed as core fluorocarbon, whereas dextran sulfate  
834 was chosen as polysaccharidic shell molecule. Vm was inserted into the outer shell throughout dextran  
835 sulfate chains. In selected experiments, VmLNBS were further functionalized by including fluorescent  
836 6-coumarin in the inner core.

837

838 **Figure 2. NB and VmLNB morphology.** NBs and VmLNBS were checked for morphology by TEM.  
839 Results are shown as representative images from three different preparations. Panel A. NB image by  
840 TEM. Panel B. VmLNB image by TEM. (see also Figure S1 in Supplementary Materials for additional  
841 images of multiple nanobubbles within the same field).

842

843 **Figure 3. Stability of Vm and VmLNB formulations.** The stability of Vm solution and VmLNB  
844 suspension was monitored up to 14 days either at room temperature (Panel A) or at 37°C (Panel B)  
845 through analysis by HPLC. Results are shown as means  $\pm$  SD from three different preparations for each  
846 formulation. Data were also analyzed for significance by ANOVA. Versus Vm solution: \*  $p < 0.001$ .

847

848 **Figure 4. Biocompatibility of Vm and VmLNBS with human keratinocytes *in vitro*.** HaCaT cells  
849 ( $10^6$  cells/2 mL DMEM medium implemented with 10% FCS) were left untreated (ctr) or treated with  
850 200  $\mu$ L of Vm solution or VmLNB suspension for 24 h in normoxia (20% O<sub>2</sub>). Thereafter, Vm and  
851 VmLNB cytotoxicity were measured through LDH assay (Panel A), whereas cell viability was  
852 measured through MTT assay (Panel B). Results are shown as means  $\pm$  SEM from three independent



853 experiments. Data were also evaluated for significance by ANOVA. No significant differences were  
854 found among all conditions.

855 **Figure 5. *In vitro* Vm release from Vm and VmLNB formulations.** Vm release from Vm solution  
856 and VmLNB suspension was monitored up to 6 h. Results are shown as means  $\pm$  SD from three  
857 different preparations for each formulation. Data were also analyzed for significance by ANOVA.  
858 Versus Vm solution: \*  $p < 0.001$ .

859

860 **Figure 6. Antibacterial activity of Vm and VmLNBS against MRSA.** MRSA were left for 2, 3, 4, 6  
861 and 24 hours at 37°C alone (ctr) or incubated with 10% v/v NBs or different concentrations of Vm,  
862 either free or loaded on VmLNBS (Panel A: 1 mg/mL; Panel B: 0.1 mg/mL; Panel C: 0.01 mg/mL;  
863 Panel D: 0.004 mg/mL). Results are shown as means  $\pm$  SEM from three independent experiments. Data  
864 on Vm- and VmLNB-treated samples were normalized upon Vm/VmLNB release ratios reported in  
865 Table 2 (see also in Supplementary Materials: Table S3 for further information on percentages of drug  
866 release from VmLNBS at different times/concentrations; and Figure S2 for raw data on VmLNB  
867 antibacterial effects). All data were also evaluated for significance by ANOVA. Versus ctr: \*  $p < 0.02$ ;  
868 versus Vm: °  $p < 0.05$ .

869

870 **Figure 7. Drug loading on dextran sulfate-shelled NBs prevents Vm internalization by MRSA.**  
871 MRSA were left alone or incubated with 10% v/v 6-coumarin-labeled VLNBS, 6-coumarin-labeled  
872 NBs, and FITC-labeled Vm for 2h at 37°C. After staining bacteria with PI, confocal fluorescent images  
873 were taken using FITC and TRITC filters. Data are shown as representative images from three  
874 independent experiments. Magnification: 100X. Red: PI. Green: 6-coumarin or FITC.

875

876 **Figure 8. US-triggered sonophoresis of VmLNBS through skin membranes.** US ( $t = 10$  min;  $f = 2.5$   
877 MHz;  $P = 5$  W) abilities to induce sonophoresis and Vm permeation from VmLNBS were evaluated up  
878 to 6 h by using a vertical diffusion Franz cell consisting in two chambers (donor and recipient,  
879 respectively) separated by a pig skin layer (see scheme in Panel A). Results are shown in Panel B as  
880 means  $\pm$  SD from three independent experiments. Data were also evaluated for significance by  
881 ANOVA. Versus without US:  $p < 0.001$ .

882 **Tables and legends**

883

Formulation	Average diameter $\pm$ SD (nm)	Polydispersity index	Zeta Potential $\pm$ SD (mV)	Viscosity (cP)
NBs	313.4 $\pm$ 26.4	0.24 $\pm$ 0.02	- 34.5 $\pm$ 0.38	1.22
VmLNBS	304.6 $\pm$ 14.6	0.22 $\pm$ 0.03	- 28.6 $\pm$ 1.34	1.25
Fluorescent NBs	312.8 $\pm$ 22.7	0.25 $\pm$ 0.02	- 34.1 $\pm$ 1.22	1.24
Fluorescent VmLNBS	308.9 $\pm$ 22.4	0.23 $\pm$ 0.01	- 29.5 $\pm$ 1.88	1.23

884

885 **Table 1. Physical-chemical characterization of NBs and VmLNBS.** Liquid formulations were  
886 characterized for average diameters, polydispersity index, and zeta potential by light scattering. The  
887 viscosity (cP) of NB and VmLNB suspensions was determined at 25 °C by using a Ubbelohde capillary  
888 viscosimeter. Results are shown as means  $\pm$  SD from three preparations. See also Figures 1-2 for  
889 further detail on NB and VmLNB structure and morphology.

890

891

892

893

894

895

896

897

time (hours)	% drug release from Vm solution	% drug release from VmLNBs	Vm/VmLNB drug release ratio
2	36.57	5.99	6.11
3	45.97	7.97	5.78
4	57.16	10.27	5.57
6	73.44	14.59	5.03
24	92.34	35.84	2.58

898

899 **Table 2. *In vitro* drug release from Vm solution and VmLNB suspension.** After incubation for  
900 increasing times (first column), the percentages of *in vitro* drug release from Vm solution (second  
901 column) and VmLNB suspension (third column) were measured. Then, Vm/VmLNB drug release  
902 ratios (fourth column) were calculated for each time considered. All incubation times (2, 3, 4, 6, and  
903 24 h) were purposely chosen to further normalize the results from the experiments with MRSA (see  
904 Figure 6). Results are shown as mean values from three different preparations for each formulation.

1 **Vancomycin-loaded nanobubbles: a new platform for controlled antibiotic delivery against**  
2 **methicillin-resistant *Staphylococcus aureus* infections.**

3

4 Monica Argenziano<sup>1</sup>, Giuliana Banche<sup>2,\*</sup>, Anna Luganini<sup>3</sup>, Nicole Finesso<sup>4</sup>, Valeria Allizond<sup>2</sup>, Giulia  
5 Rossana Gulino<sup>4</sup>, Amina Khadjavi<sup>4,5</sup>, Rita Spagnolo<sup>1</sup>, Vivian Tullio<sup>2</sup>, Giuliana Giribaldi<sup>4</sup>, Caterina  
6 Guiot<sup>5</sup>, Anna Maria Cuffini<sup>2</sup>, Mauro Prato<sup>2,5,§</sup>, Roberta Cavalli<sup>1, §,\*</sup>

7

8 <sup>1</sup> *Dipartimento di Scienza e Tecnologia del Farmaco, Università degli Studi di Torino, Torino, Italy*

9 <sup>2</sup> *Dipartimento di Scienze della Sanità Pubblica e Pediatriche, Università degli Studi di Torino, Torino,*  
10 *Italy*

11 <sup>3</sup> *Dipartimento di Scienze della Vita e Biologia dei Sistemi, Università degli Studi di Torino, Torino,*  
12 *Italy*

13 <sup>4</sup> *Dipartimento di Oncologia, Università degli Studi di Torino, Torino, Italy*

14 <sup>5</sup> *Dipartimento di Neuroscienze, Università degli Studi di Torino, Torino, Italy*

15 *§ Equal contribution to the work*

16 *\* Corresponding authors:*

17 Prof. Roberta Cavalli, Dipartimento di Scienza e Tecnologia del Farmaco, Università degli Studi di  
18 Torino, via P. Giuria 9, 10125 Torino, Italy. Phone no.: +39-011-6707686. Fax no.: +39-011-6707687.

19 E-mail address: [roberta.cavalli@unito.it](mailto:roberta.cavalli@unito.it)

20 Dr. Giuliana Banche, Dipartimento di Scienze della Sanità Pubblica e Pediatriche, Università degli  
21 Studi di Torino, Via Santena 9, 10126 Torino, Italy. Phone no.: +39-011-6705627. Fax no.: +39-011-  
22 2365627. E-mail address: [giuliana.banche@unito.it](mailto:giuliana.banche@unito.it)

23 **Abstract**

24

25 Vancomycin (Vm) currently represents the gold standard against methicillin-resistant *Staphylococcus*  
26 *aureus* (MRSA) infections. However, it is associated with low oral bioavailability, formulation stability  
27 issues, and severe side effects upon systemic administration. These drawbacks could be overcome by  
28 Vm topical administration if properly encapsulated in a nanocarrier. Intriguingly, nanobubbles (NBs)  
29 are responsive to physical external stimuli such as ultrasound (US), promoting drug delivery. In this  
30 work, perfluoropentane (PFP)-cored NBs were loaded with Vm by coupling to the outer dextran sulfate  
31 shell. Vm-loaded NBs (VmLNBS) displayed ~300 nm sizes, anionic surfaces and good drug  
32 encapsulation efficiency. *In vitro*, VmLNBS showed prolonged drug release kinetics, not accompanied  
33 by cytotoxicity on human keratinocytes. Interestingly, VmLNBS were generally more effective than  
34 Vm alone in MRSA killing, with VmLNB antibacterial activity being more sustained over time as a  
35 result of prolonged drug release profile. Besides, VmLNBS were not internalized by *staphylococci*,  
36 opposite to Vm solution. Further US association promoted drug delivery from VmLNBS through an *in*  
37 *vitro* model of porcine skin. Taken together, these results support the hypothesis that proper Vm  
38 encapsulation in US-responsive NBs might be a promising strategy for the topical treatment of MRSA  
39 wound infections.

40

41 **Key words**

42 Nanobubbles; vancomycin; methicillin-resistant *Staphylococcus aureus*; ultrasound; prolonged release.

43

## 44 **1. Introduction**

45

46 Chronic wounds fail to proceed through timely regulated and interrelated processes to restore  
47 anatomical and functional integrity of the injured tissues (Lazarus et al., 1994) such as diabetic feet,  
48 bedsores, and venous ulcers (Markova et al., 2012). To date, these types of wounds are considered like  
49 a silent epidemic, affecting a large fraction of the world population and posing a major gathering threat  
50 to the public health and economy of all developed countries (Daeschlein, 2013). Hospitalized patients  
51 are at particular risk, especially those suffering from diabetes, human immunodeficiency virus or other  
52 immune disorders, as well as those undergoing chemotherapy (Payne et al., 2008).

53 Beyond delayed healing processes due to different factors (hypoxia, persistent inflammation, and  
54 altered balances between tissue remodelling proteinases and their inhibitors), chronic wounds are often  
55 worsened by microbial infections (Gurusamy et al., 2013). Among the bacteria responsible for skin  
56 infection, *Staphylococcus aureus* represents the most common pathogen to be identified in chronic  
57 wounds, with methicillin-resistant *S. aureus* (MRSA) accounting for upward of 20% to 50% of cases  
58 (Price, 2010). MRSA colonies often develop at the interface between synthetic prostheses and  
59 biological tissues, particularly during surgery and post-surgery course. In addition, MRSA colonization  
60 or infection of wounds can result in MRSA bacteremia, which is associated with a 30-day mortality of  
61 about 28% to 38% patients (Gurusamy et al., 2013).

62 The main goal of chronic wound treatment is to decrease the injuring-associated microbial load, thus  
63 allowing wound healing processes to take place. However, conventional systemic delivery of  
64 antibiotics not only entails poor penetration into ischemic and necrotic tissues, but can also cause  
65 systemic toxicity with associated renal and liver complications, resulting in forced hospitalization for  
66 further monitoring and advanced treatment. On the contrary, topically applied antimicrobials have

67 | proven effective in decreasing bacterial levels in granulating wounds (Diehr et al., 2008~~7~~). Therefore,  
68 | alternative local delivery of antimicrobials - either by topical administration or through novel delivery  
69 | devices - may enable to keep high local antibiotic concentrations for prolonged release times without  
70 | reaching systemic toxicity (Zilberman et al., 2008).

71 | A promising approach to develop a topical therapy for microbial infection in skin and soft tissues  
72 | would employ biocompatible nanomaterials and drug nanocarriers. Indeed, nanotechnology represents  
73 | an emerging field to be exploited for antibiotic drug delivery. Thanks to their physical and chemical  
74 | properties (small size, high surface-to-volume ratio and suitable surface modification) nano-sized  
75 | materials may be used as drug carriers to trespass several physiological barriers and to reach biological  
76 | targets. The coupling of nanocarriers with anti-infectious agents makes it likely to increase drug  
77 | concentrations and drug penetration at the site of infection. As a result, it might not only improve the  
78 | therapeutic index but also reduce some issues associated with nonspecific cytotoxicity and antibiotic  
79 | resistance (Sharma et al., 2012).

80 | Vancomycin hydrochloride, being effective against many Gram-positive bacteria that are unresponsive  
81 | to common antibiotics, represents the gold standard against MRSA infections (Kullar~~rrant~~ et al., 2016).  
82 | However, Vm is poorly absorbed from the gastrointestinal tract with a low oral bioavailabiliy. Low  
83 | intravenous infusion is often suggested as a feasible alternative for drug administration, but Vm  
84 | instability in aqueous solutions at 37°C could imply a tremendous reduction of drug effectiveness  
85 | (Mawhinney et al., 1992; Raverdy et al., 2013). Following parenteral administration, Vm displays a  
86 | slow mode of action, a complex concentration-time profile, and a disappointingly low penetration in  
87 | tissues (Vandecasteele et al., 2012). Furthermore, systemic Vm administration can be associated with  
88 | several adverse effects (Vidal et al., 1992). On the other hand, Vm topical application – that would be  
89 | much safer than systemic administration - is currently limited by several factors such as skin barrier  
90 | properties and poor drug permeability (Giandalia et al., 2001). Being the main goal of chronic wound



91 treatment to decrease the microbial load, allowing the healing processes to take place, new delivery  
92 protocol should be devised, since conventional systemic delivery of antibiotics requires a drug  
93 concentration which is locally ineffective because of the poor penetration into ischemic and necrotic  
94 tissues, but can cause systemic toxicity and topically applied antimicrobials have proven effective in  
95 decreasing bacterial levels in granulating wounds (Diehr et al., 2007), without inducing systemic  
96 toxicity (Zilberman et al., 2008) but suffer from poor diffusion across membranes.

97 Intriguingly, the use of a nanocarrier may help to avoid the abovementioned drawbacks. Notably,  
98 nanocarriers such as liposomes, microemulsions, and lipid nanoparticles have the potential to deliver  
99 drugs to the skin more efficiently than conventional topical carriers such as creams and ointments, that  
100 are not usually recommended for applications on injured skin (Giandalia et al., 2001; Prabhu et al.,  
101 2012). However, the response to drug topical applications has been too weak so far, mainly due to the  
102 inability to cross the external skin barrier (*stratum corneum*) and reach the dermal regions where the  
103 bacteria are nested. Interestingly, physical media such as ultrasound (US) are reportedly able to trigger  
104 drug release at the site of infection by temporarily increasing skin permeability through sonophoresis.  
105 As such, US is useful to promote drug targeting and transdermal delivery in a non-invasive manner  
106 (Azagury et al., 2014; Park et al., 2012).

107 Microbubbles (MBs) (Guiot et al., 2006), nanobubbles (NBs) (Cavalli et al., 2009a; Cavalli et al.,  
108 2009b; Cavalli et al., 2016) and nanodroplets (NDs) (Magnetto et al., 2014; Prato et al., 2015) are  
109 suitable carriers to be combined with such a physical trigger. They are spherical core-shell structures  
110 filled with gases such as perfluorocarbons. Particularly, oxygen-cored nanostructures can be employed  
111 both for sonography (as contrast agents) (Fokong et al., 2012; Marxer et al., 2011) and for therapy (as  
112 hypoxia- and infection-counteracting devices) (Gulino et al., 2015; Banche et al., 2015; Khadjavi et al.,  
113 2015; Basilico et al., 2015; Prato et al., 2016). In particular NBs, consisting in an outer shell of a  
114 biocompatible/biodegradable polysaccharide (chitosan, dextran, or dextran sulfate) and an inner core

115 filled with an oxygen-storing fluorocarbon (perfluoropentane, PFP), have been purposely developed as  
116 a new non-invasive, low-cost and multipurpose nanotechnological platform (Cavalli et al., 2009a;  
117 Cavalli et al., 2009b; Cavalli et al., 2016). PFP is a perfluorocarbon with a boiling point of 29°C, hence  
118 liquid at room temperature. The use of PFP allows liquid droplet generation at room temperature. Then,  
119 PFP in nanodroplets can be activated by an external stimulus, like US, by means of a mechanism called  
120 acoustic droplet vaporization, causing the droplet to become a bubble. Depending on the properties of  
121 the nanostructure, NBs can be subsequently coupled with different molecules, such as drugs or genetic  
122 materials, thus acting as nanocarriers (Cavalli et al., 2012; Cavalli et al., 2013; Delalande et al., 2012;  
123 Yin et al., 2014). Due to their structure and their gaseous core, NBs are very responsive to US and can  
124 take advantage from a number of effects related to microcavitation and microstreaming, occurring at  
125 the liquid-membrane interface and responsible for transitory and reversible openings of the pores, thus  
126 crossing the membrane itself and delivering their content beyond the tissue (sonophoresis) or the cell  
127 (sonoporation) membrane (Karshafian et al., 2009).

128 Based on these preconditions, the present work aimed at producing dextran sulfate-shelled and PFP-  
129 cored NBs for Vm local delivery to potentially treat skin infectious diseases. The formulation is  
130 referred to as “nanobubbles” for sake of simplicity but it must be said that, prior to the application of  
131 US, it would be more accurate to use the term “nanodroplets” when the core is constituted of PFP.  
132 Therefore, Vm-loaded NBs (VmLNBs) were prepared and characterized for physico-chemical  
133 parameters and drug release kinetics; tested for biocompatibility with human skin cells and for their  
134 antibacterial properties or interactions with MRSA; and challenged for responsiveness to US, in order  
135 to assess their effectiveness as Vm nanocarriers for local delivery.

136

137 **2. Material and methods**

138

139 **2.1. Materials**

140 All materials were from Sigma-Aldrich, St Louis, MO, unless those indicated as follows. Sterile  
141 plastics were from Costar, Cambridge, UK; ethanol (96%) was from Carlo Erba (Milan, Italy); soybean  
142 lecithin (Epikuron 200<sup>®</sup>) was from Cargill (Hamburg, Germany); 1-800 Millipore system to obtain  
143 ultrapure water and Amicon<sup>®</sup> Ultra-0.5 centrifugal filter device were from Millipore (Molsheim,  
144 France); Ultra-Turrax SG215 homogenizer was from IKA (Staufen, Germany); RPMI 1640 medium  
145 was from Invitrogen (Carlsbad, CA); Nanobrook 90Plus Particle Size Analyzer was from Brookhaven  
146 (New York City, NY); Philips CM10 electron microscope was from Philips (Eindhoven, the  
147 Netherlands); Ubbelohde capillary viscosimeter was from SCHOTT Instruments GmbH (Mainz,  
148 Germany); Perkin Elmer PUMP 250B was from Perkin Elmer (Waltham, MA); Flexar UV/Vis LC  
149 spectrophotometer detector was from Perkin Elmer (Waltham, MA); Agilent TC C<sub>18</sub> columns were  
150 from Agilent (Santa Clara, CA); Orion Model 420A pH Meter was from Thermo Scientific (Waltham,  
151 MA); Semi-Micro Osmometer K-7400 was from Knauer (Berlin, Germany); Beckman Coulter Allegra  
152 64R Centrifuge was from Beckman Coulter (Brea, CA); Spectra/Por cellulose membranes were from  
153 Spectrum Laboratories (Rancho Dominguez, CA); HaCaT cells were from Cell Line Service GmbH  
154 (Eppelheim, Germany); cell culture RPMI 1640 and Dulbecco's modified Eagle's medium (DMEM)  
155 were from Invitrogen (Carlsbad, CA); streptomycin was from Cambrex Bio Science (Vervies,  
156 Belgium); humidified CO<sub>2</sub>/air-incubator was from Thermo Fisher Scientific Inc. (Waltham, MA);  
157 tryptic soy broth (TSB) and tryptic soy agar (TSA) were from Merk KgaA (Darmstadt, Germany);  
158 Olympus Fluoview 200 laser scanning confocal system mounted on an inverted IX70 Olympus  
159 microscope was from Olympus America Inc. (Melville, NY, USA) ; SPSS 16.0 software was from  
160 SPSS Inc. (Chicago, IL).

161

## 162 **2.2. Development and manufacturing of formulations**

163

### 164 **2.2.1. Determination of Vm and dextran sulfate interaction ratio**

165 Increasing concentrations (0.25, 0.5, 1.0, 2.0 mg/mL) of dextran sulfate aqueous solutions (1 mL) were  
166 added to 1 mL of Vm aqueous solution (1 mg/mL) under magnetic stirring at room temperature  
167 overnight. After equilibration, the systems were separated by centrifugation (20000 rpm, 15 minutes)  
168 using a centrifugal filter device (Amicon<sup>®</sup> Ultra), in order to determine the amount of unbound Vm in  
169 the filtrate phase. The drug concentration in the filtrate was determined using the HPLC method  
170 described below.

171

### 172 **2.2.2. Preparation of NB, Vm, and VmLNB formulations**

173 NBs were formulated using PFP for the inner core and dextran sulfate for the shell. A purposely tuned  
174 multi-step protocol was designed. Briefly, a pre-emulsion was obtained adding 300 μmL of an ethanol  
175 solution containing Epikuron<sup>®</sup> 200 and palmitic acid (1% w/v) to 500 μL of PFP under magnetic  
176 stirring. After the addition of 4.8 mL of ultrapure water, the system was homogenized using a Ultra-  
177 Turrax SG215 homogenizer. To obtain the polymeric NBs, 350 μL of 1% w/v dextran sulfate  
178 (molecular weight = 100 kDa) aqueous solution was added drop-wise under magnetic stirring. Blank  
179 NBs obtained according to this procedure were employed as control formulations in the subsequent  
180 experiments. On the other hand, to obtain VmLNBs, an extra step based on drop-wise addition of a Vm  
181 aqueous solution (pH 3.5) to the so-formed NBs was performed under mild stirring. Different  
182 concentrations of Vm solutions were added to prepare a series of VmLNB formulations with increasing  
183 drug content (0.004, 0.01, 0.1, and 1 mg/mL). VmLNBs were then purified by dialysis to eliminate

184 unbound molecules. For selected experiments, fluorescent NBs and VmLNBS were obtained by the  
185 addition of 6-coumarin (1 mg/mL) to the PFP core. Alternatively, fluorescent Vm was synthesized  
186 through reaction between fluorescein isothiocyanate (FITC) and Vm. For this purpose, an amount of  
187 FITC solution in methanol (0.2 % w/v) was added to Vm aqueous solution and incubated under stirring  
188 overnight in the dark. **Figure 1** shows a representative scheme resuming the general structure of  
189 fluorescent VmLNBS. For cell experiments, NBs were prepared in phosphate buffer saline pH 7.4  
190 (PBS). For *in vitro* permeation studies, NBs were prepared in saline solution (NaCl 0.9% w/v).

Formatted: Font: Italic

191

### 192 **2.2.3. NB sterilization**

193 Firstly, the glassware and the components were sterilized at 121 °C and 2 bar. Subsequently, all NB  
194 formulations were sterilized through UV-C exposure for 20 min. Thereafter, UV-C-treated materials  
195 were incubated with cell culture RPMI 1640 medium in a humidified CO<sub>2</sub>/air-incubator at 37°C up to  
196 72 h, not displaying any signs of microbial contamination when checked by optical microscopy.

197

## 198 **2.3. Characterization of formulations**

199

### 200 **2.3.1. Characterization of NB and VmLNB formulations**

201 The average diameter, polydispersity index and zeta potential were determined by photocorrelation  
202 spectroscopy using a particle size analyzer at a scattering angle of 90° and a temperature of 25 °C. NB  
203 suspensions were diluted in deionized filtered water before measurement. For zeta potential  
204 determination, samples of diluted NB formulations were placed in the electrophoretic cell, where an  
205 electric field of approximately 15 V/cm was applied. The morphology of formulations was evaluated  
206 by Transmission Electron Microscopy (TEM), using a Philips CM10 (Eindhoven, NL) instrument. NB  
207 and VmLNB aqueous suspensions were sprayed on Formwar-coated copper grid and air-dried before

208 observation. The viscosity of the samples was determined at 25 °C using a Ubbelohde capillary  
209 viscosimeter.

210

### 211 **2.3.2. HPLC quantitative Vm determination**

212 Vm quantitative determination was carried out by using an HPLC system based on a Perkin Elmer  
213 pump equipped with a spectrophotometer detector. Analyses were performed using an Agilent TC C<sub>18</sub>  
214 column (250 mm × 4.6 mm, 5 µm). The mobile phase was a mixture of KH<sub>2</sub>PO<sub>4</sub> 50 mM (pH 4) and  
215 acetonitrile (92:8 v/v), degassed and pumped through the column with a flow rate of 1 mL/min.  
216 Ultraviolet detection was set at 286 nm. The external standard method was used to calculate the drug  
217 concentration. For this purpose, 1 mg of Vm was weighted, placed in a volumetric flask, and dissolved  
218 in water to obtain a stock standard solution. This solution was then diluted using the mobile phase,  
219 providing a series of calibration solutions, subsequently injected into the HPLC system. Linear  
220 calibration curve was obtained over the concentration range of 0.5–25 µg/mL, with a regression  
221 coefficient of 0.999.

222

### 223 **2.3.3. In vitro evaluation of Vm stability**

224 Vm chemical stability - either solved in aqueous solution or loaded in VmLNBS - was evaluated at  
225 room temperature and at 37 °C over time. A quantitative determination of Vm concentration over time  
226 was carried out using the HPLC method described above.

227

### 228 **2.3.4. NB stability over time and after US administration**

229 The physical stability of NBs was evaluated by morphological analysis and by size and zeta potential  
230 determination of formulation over time. Their average diameters, zeta potential values and morphology  
231 were assessed up to six months. Stability was also investigated following NB exposure to US ( $f = 2.5 \pm$

232 0.1 MHz; t = 10 min; P = 5 W). NB morphology was observed by TEM to confirm the integrity of NB  
233 structure.

234

### 235 **2.3.5. Encapsulation efficiency and loading capacity of Vm in NBs**

236 The encapsulation efficiency of VmLNBS was determined using a centrifugal filter system. 150  
237 ~~µ~~µmL of VmLNB suspension were put in an Amicon® Ultra-0.5 centrifugal filter device and  
238 centrifuged at 15000 rpm for 30 minutes using Beckman Coulter Allegra 64R Centrifuge. The solution  
239 filtered in the bottom of the tube was quantified and after suitable dilution was analyzed by HPLC, in  
240 order to obtain the concentration of free Vm in VmLNBS suspensions. The encapsulation efficiency  
241 was calculated by subtracting the amount of free drug from the initial amount of added Vm, according  
242 to the following equation:

$$243 \text{ Encapsulation efficiency} = \frac{(\text{total Vm} - \text{free Vm})}{\text{total Vm}} \times 100$$

244 The loading capacity was determined on freeze-dried NB samples. Briefly, a weighted amount of  
245 freeze-dried VmLNBS was ~~suspended~~ ~~diluted~~ in 105 mL of water. After sonication and centrifugation,  
246 the supernatant was diluted with mobile phase and analyzed by HPLC. The loading capacity of Vm in  
247 VmLNBS was calculated as follows:

$$248 \text{ Loading capacity} = \frac{(\text{total Vm} - \text{free Vm})}{\text{NB weight}} \times 100$$

249

### 250 **2.4. In vitro release studies**

251 *In vitro* drug release experiments were conducted in a multi-compartment rotating cell, comprising a  
252 donor chamber separated by a cellulose membrane (cut-off = 12000 Da) from a receiving compartment.  
253 One ml of VmLNB suspension at different concentrations (1, 0.1, 0.01 and 0.004 mg/mL) was placed

254 in the donor chamber. The *in vitro* release kinetics of Vm from VmLNB was compared to a Vm  
255 aqueous solution (1 mg/mL) as a control. The receiving phase, containing phosphate buffer 0.05 M (pH  
256 7.4) was withdrawn at regular intervals and replaced with the same amount of fresh buffer. Quantitative  
257 determination of Vm in the withdrawn samples was carried out by the HPLC method, as described in  
258 the previous paragraph. Data were expressed as % of Vm released over time.

259

## 260 **2.5. *In vitro* permeation study**

261 *In vitro* studies were performed using a vertical diffusion Franz cell to evaluate Vm permeation  
262 throughout the skin. The Franz cell consists of a donor compartment, with Vm (1 mg/mL, either free or  
263 carried by VmLNBS,  $1 \times 10^{12}$  NBs/ml) and a receiving compartment containing 0.9% w/w NaCl saline  
264 solution. To simulate the *stratum corneum* properties a membrane pig ear skin was used. Skin slices  
265 were isolated with a dermatome from the outer side of pig ears, obtained from a local slaughterhouse,  
266 and then were frozen at  $-18$  °C. Before starting the experiments, the skin was equilibrated in NaCl 0.9  
267 % w/w saline solution, in the presence of 0.01% sodium azide to preserve the skin, at 25 °C for 30 min.  
268 Then, after washing with saline solution, the skin layer was inserted between the two compartments of  
269 the Franz cell, with the stratum corneum side facing towards the donor chamber. The study was carried  
270 out for 24 hours and the receiving phase was withdrawn at regular times and replaced with the same  
271 amount of fresh receiving medium. The collected samples were then analyzed by HPLC to determine  
272 the amount of Vm permeated over time. US abilities to promote Vm permeation were also investigated.  
273 For this purpose, a high frequency US transducer ( $f = 2.5$  MHz;  $P = 5$  W;  $t = 10$  min) was combined to  
274 a purposely modified vertical diffusion cell. Drug permeation through pig skin after US application was  
275 monitored by HPLC analysis of the cumulative amount of antibiotic reaching the receiving phase over  
276 time.

277

Formatted: Superscript

Formatted: Font: Italic



278 **2.6. Human biocompatibility studies**

279

280 **2.6.1. Human keratinocyte cell cultures**

281 HaCaT, a long-term cell line of human keratinocytes immortalized from a 62-year old Caucasian male  
282 donor (Boukamp et al., 1988), was used for the assessment of Vm and VmLNB biocompatibility. Cells  
283 were grown as adherent monolayers in DMEM medium supplemented with 10% fetal bovine serum,  
284 100 U/mL penicillin, 100 µg/mL streptomycin and 2 mM L-glutamine in a humidified CO<sub>2</sub>/air-  
285 incubator at 37°C. Before starting the experiments, cells were washed with PBS, detached with  
286 trypsin/ethylenediaminetetraacetic acid (0.05/0.02 % v/v), washed with fresh medium and plated at a  
287 standard density (10<sup>6</sup> cells/well in 6-well plates) in 2 mL of fresh medium.

288

289 **2.6.2. Vm and VmLNB cytotoxicity**

290 The potential cytotoxic effects of VmLNBS were measured as the release of lactate dehydrogenase  
291 (LDH) from HaCaT cells into the extracellular medium. Briefly, cells were incubated in DMEM  
292 medium for 24 h with/without 1 mg/mL Vm, either free or carried by VmLNBS, in a humidified  
293 CO<sub>2</sub>/air-incubator at 37°C. Then, 1 mL of cell supernatants was collected and centrifuged at 12000  
294 rpm+3000g for 2 min. Cells were washed with fresh medium, detached with  
295 trypsin/ethylenediaminetetraacetic acid (0.05/0.02 % v/v), washed with PBS, resuspended in 1 mL of  
296 TRAP (82.3 mM triethanolamine, pH 7.6), and sonicated on ice with a 10 s burst. 5 µmicroL of cell  
297 lysates and 50 microL of cell supernatants were diluted with TRAP and supplemented with 0.5 mM  
298 sodium pyruvate and 0.25 mM NADH (300 µmicroL as a final volume) to start the reaction. The  
299 reaction was followed measuring the absorbance at 340 nm (37 °C) with Synergy HT microplate  
300 reader. Both intracellular and extracellular enzyme activities were expressed as µmol of oxidized

301 NADH/min/well. Finally, cytotoxicity was calculated as the net ratio between extracellular and total  
302 (intracellular + extracellular) LDH activities.

303

### 304 **2.6.3. Human keratinocyte cell viability**

305 Cell viability was evaluated using 3-(4,5-dimethylthiazol-2-yl)-2,5-diphenyltetrazolium bromide  
306 (MTT) assay. HaCaT cells were incubated for 24 h with/without 1 mg/mL Vm, either free or carried by  
307 VmLNBS, in a humidified CO<sub>2</sub>/air-incubator at 37°C. Thereafter, 20 ~~micro~~μL of 5 mg/mL MTT in  
308 PBS were added to cells for 3 additional hours at 37 °C. The plates were then centrifuged, the  
309 supernatants discarded and the dark blue formazan crystals dissolved using 100 μL of lysis buffer  
310 containing 20 % (w/v) sodium dodecyl sulfate, 40 % N,N-dimethylformamide (pH 4.7 in 80 % acetic  
311 acid). The plates were then read on Synergy HT microplate reader at a test wavelength of 550 nm and  
312 at a reference wavelength of 650 nm.

313

## 314 **2.7. Microbiological assays**

315

### 316 ***2.7.1. Determination of vancomycin antimicrobial activity against MRSA***

317 Vm solutions were freshly prepared for each experiment. Determination of the minimum inhibitory  
318 concentration (MIC) of vancomycin was carried by the microdilution broth method according to the  
319 latest Clinical and Laboratory Standards Institute (CLSI) guidelines (CLSI 2012). Interpretation of the  
320 results was performed as outlined in the above mentioned CLSI guidelines (CLSI 2012).

321

### 322 ***2.7.2. In vitro antibacterial efficiency of VmLNBS against MRSA.***

323 MRSA, isolated from human ulcerated wounds (Infermi Hospital, Biella, Italy), was cultured over  
324 night at 37°C in TSB. After incubation, bacteria were re-suspended in 100 mL of TSB, harvested by 10

325 min centrifugation at 4,000 rpm, diluted in TSB to  $10^4$  colony-forming-unit (CFU)/mL, as confirmed  
326 by colony counts on TSA, and then incubated in TSB with VmLNBS, loaded with Vm at different  
327 concentrations (1, 0.1, 0.01, and 0.004 mg/mL), in sterile sampling tubes for 2, 3, 4, 6, and 24 hours at  
328 37°C. Controls represented by either bacteria incubated in TSB, bacteria incubated with blank NBs or  
329 bacteria incubated in the presence of free Vm at different concentrations (1, 0.1, 0.01 and 0.004  
330 mg/mL), were also performed. At each incubation time, serial 10-fold dilutions in saline solution (0.9%  
331 NaCl) were prepared from each sample, and 100 ~~umiero~~  $\mu$ L of each dilution were spread on TSA, so that  
332 the number of CFU/mL could be determined.

333

### 334 **2.7.3. Imaging with confocal laser scanning microscopy**

335 ~~MRSA bacteria S. aureus strain~~ ~~were~~ ~~was~~ grown in TSB at 37°C in agitation until reaching the  
336 concentration of  $1 \times 10^9$  CFU/mL. Then, 1 mL aliquot of bacteria was pelleted (3000g x 10 min at  
337 4°C), resuspended in PBS 1x and incubated with 6-coumarin-labeled VmLNBS, 6-coumarin-labeled  
338 NBs, or FITC-labeled Vm at a dilution of 1:11, as for previous experiments performed on eukaryotic  
339 cells. Each sample was placed on orbital shaker (160 rpm) in the dark at 37°C for 2h and 4h. After  
340 incubation, one drop from each suspension was streaked on poly-L-lysine-coated microscope slides and  
341 allowed to dry. Then, bacteria were stained with iodide propidium (PI) in PBS 1X and again allowed to  
342 dry. Fluorescence images were taken with an Olympus IX70 inverted laser scanning confocal  
343 microscope, and captured using FluoView 200 software.

344

### 345 **2.8. Statistical analysis**

346 At least three independent experiments, each one in duplicate or triplicate, were performed for every  
347 investigational study. Numerical data are shown as means  $\pm$  SEM for inferential results or as means  $\pm$   
348 SD for descriptive results (see Cumming et al., 2007 for an exhaustive review). Imaging data are shown

349 as representative pictures. All data were analyzed by a one-way Analysis of Variance (ANOVA)  
350 followed by Tukey's post-hoc test (software: SPSS 16.0 for Windows, SPSS Inc., Chicago, IL).  $P < 0.05$   
351 were considered significant.

352

353 **3. Results**

354

355 **3.1. Characterization of VmLNB and control (blank NB and Vm) formulations**

356 Before NB production, the interaction between dextran sulfate and Vm was firstly investigated to  
357 optimize Vm/dextran sulfate ratio. Results indicated that Vm was complexed at 99% by dextran sulfate  
358 solution until the concentration of 0.5 mg/mL (data not shown). The Vm/dextran sulfate ratio was  
359 calculated corresponding to 2:1 (w/w). Based on this preliminary information, NBs were prepared  
360 according to the protocol described in the Materials and Methods section. After manufacturing,  
361 VmLNB and blank NB formulations (with or without 6-coumarin in the inner core) were characterized  
362 physico-chemically. Results are shown in **Figure 2** and **Tables 1-2**. Both VmLNBs and NBs displayed  
363 spherical shapes with a core-shell structure by TEM analyses. All sizes were in the nanometer range,  
364 with all formulations displaying around 300 nm as a value for average diameters. All polydispersity  
365 indexes were included between 0.22 and 0.25. Zeta potentials ranged from -34 mV (NBs) to -29 mV  
366 (VmLNBs). ~~The loading of Vm in the NB structure did not significantly affect the viscosity of the  
367 formulations. NB viscosity (1.12 cP) was slightly increased upon binding with Vm (1.25 cP for  
368 VmLNBs).~~ NBs were able to load Vm with an encapsulation efficiency of 86% and loading capacity of  
369 29%.

370

371 **3.2. Stability of VmLNB and control (blank NB and Vm) formulations**

372 NB and VmLNB formulations proved to be physically stable over time, as confirmed by long-term  
373 checking of the parameters assessed in the previous paragraph. Indeed, the obtained values did not  
374 remarkably change up to six months after the manufacturing of the formulations stored at 4 °C (data  
375 not shown). Furthermore, the chemical stability of the drug was comparatively checked between free  
376 Vm solution and VmLNB aqueous suspension either over time (up to 14 days) or at different

377 temperatures (25°C and 37°C). As shown in **Figure 3**, ~~the drug Vm always~~ resulted much more stable  
378 from a chemical point of view when properly incorporated in the nanocarriers (VmLNBS) than as such  
379 in solution alone.

380

### 381 **3.3. Human biocompatibility**

382

383 The potential toxicity of Vm solution and VmLNB suspension on human skin cells was assessed by  
384 testing *in vitro* cultured HaCaT keratinocytes. Cells were incubated for 24 h alone, with 10% v/v Vm  
385 solution, or with VmLNB nanosuspensions in normoxic conditions (20% O<sub>2</sub>). Thereafter, cytotoxicity  
386 was analyzed by LDH assay, and cell viability by MTT assay. As shown in **Figure 4**, neither Vm nor  
387 VmLNBS did show significant toxic effects and HaCaT cell viability was not significantly affected by  
388 either formulation.

389

### 390 **3.4. *In vitro* drug release from VmLNBS**

391 *In vitro* drug release from VmLNB nanosuspension and free Vm solution were comparatively  
392 evaluated over time. As shown in **Figure 5** (time course studies up to 6 h) and **Table 23** (end-point data  
393 up to 24 h), 1 mg/mL Vm release from VmLNBS was slow and prolonged over time, compared to free  
394 drug solution diffusion. No initial burst effect was observed indicating Vm incorporation in NB shell.  
395 Further information on additional incubation times and drug concentrations for VmLNBS is available in  
396 Supplementary Materials (**Table S31**). Vm/VmLNB drug release ratios at different times (2, 3, 4, 6,  
397 and 24 h) were also calculated (see **Table 23**), in order to allow normalization of the results from  
398 treatment with VmLNBS in the microbiological experiments described in the following paragraph.

399

### 400 **3.5. *In vitro* antimicrobial activity of VmLNBS**

401 According to preliminary microbiological analyses performed on the MRSA strain employed in the  
402 present experiments, 0.004 mg/mL resulted as the MIC value for Vm. Therefore, decreasing Vm  
403 concentrations from 1 mg/mL (used for the studies described in the previous paragraphs) to 0.004  
404 mg/mL (MIC value) were employed in a series of experiments aimed at comparatively evaluating Vm  
405 (either free or carried by VmLNBS) antibacterial effectiveness against MRSA. Bacteria were incubated  
406 at different times (2, 3, 4, 6, and 24 h) either alone (ctr) or with free Vm, VmLNBS, or blank NBs. The  
407 initial drug concentrations (1; 0.1; 0.01; and 0.004 mg/mL) loaded on VmLNBS were the same as those  
408 solved in free Vm solution. However, as emerged in the previous paragraph, drug release from  
409 VmLNBS is significantly slower than free Vm solution diffusion. For this reason, before proceeding  
410 with the analysis of the results, all values on bacterial growth referring to Vm- and VmLNB-treated  
411 samples were normalized upon time-dependent Vm/VmLNB drug release ratios shown in **Table 23**.  
412 Normalized results are shown in **Figure 6**, whereas raw data are available in Supplementary Materials  
413 (**Figure S24**). 1 mg/mL Vm effectively inhibited bacterial growth at all times, independently from  
414 being free or carried by the nanocarrier. Lower drug concentrations of free Vm solution were effective  
415 against MRSA only after longer times of incubation (at least 3 h for 0.1 mg/mL and 0.01 mg/mL Vm;  
416 and at least 4 h for 0.004 mg/mL Vm). Interestingly, Vm antibacterial efficacy was significantly  
417 improved when the drug was carried by VmLNBS. Indeed, VmLNB-dependent inhibition of bacterial  
418 growth was significantly enhanced compared to free Vm solution, at all drug concentrations.  
419 Additionally, compared to free Vm solution, VmLNB antibacterial effects appeared earlier, as they  
420 were already evident after 2 h of incubation (the first time-point of the observational period) at all Vm  
421 concentrations. Blank NBs did not show any antibacterial activity.

422 Further analysis by confocal microscopy (**Figure 7**) displayed that MRSA avidly internalized free  
423 fluorescent Vm already after 2 h of incubation, but not fluorescent VmLNBS. Fluorescent Vm-free NBs  
424 did adhere to the bacterial cell wall without being internalized.

425 **3.6. US-triggered drug permeation**

426 The ability of US to promote Vm permeation through the skin was assayed by employing a purposely  
427 modified Franz cell constituted by a donor and a recipient chamber separated by a pig skin layer (see  
428 **Figure 8A** for a schematic representation of the apparatus). As shown in **Figure 8B**, the administration  
429 of US (t = 10 min; f = 2.5 MHz; P = 5 W) strongly induced VmLNBS to deliver the antibiotic drug  
430 from the donor chamber throughout the pig skin membrane into the recipient chamber up to 6 h.  
431 Furthermore, drug accumulated in the skin after US treatment reached 158  $\mu\text{g}/\text{cm}^2$  after 6 hours.

432

433

434

435



#### 436 4. Discussion

437

438 Vm currently represents the main stay against MRSA infections ([Koyama et al., 2013](#); ~~Kullar et al., 2016~~)  
439 al., 2016). However, Vm administration raises several issues that urgently need to be faced, including  
440 its marked instability, low oral bioavailability, complex concentration-time profile, low tissue  
441 penetration (ranging from 10% in diabetic to 30% in normal skin and soft tissues), and several adverse  
442 effects (Mawhinney et al., 1992; Raverdy et al., 2013; Vandecasteele et al., 2012; Vidal et al., 1992;  
443 Giandalia et al., 2001). In the attempt to counteract these drawbacks, thus improving the effectiveness  
444 of Vm delivery, some novel nanocarriers have been developed: i) Vm coupling to chitosan as an ocular  
445 drug delivery vehicle for topical use in rabbit eyes has appeared more effective than carrier-free Vm  
446 (Khangtragool et al., 2011); ii) PEGylated liposomal Vm enhanced the effective treatment of MRSA  
447 pneumonia and simultaneously reduced the nephrotoxicity risk compared with conventional and non-  
448 PEGylated Vm formulations (Muppidi et al., 2011); iii) Vm-loaded liposomes, stabilized with chitosan  
449 modified gold nanoparticles bounded to their surface, have proven effective in inhibiting the bacterial  
450 growth (Pornpattananangkul et al., 2011); and iv) Vm-containing trehalose and hydroxyethylcellulose  
451 spherical matrices have been developed as new delivery systems suitable for topical applications on  
452 extensive and purulent wounds (Giandalia et al., 2001). Recently, Vm-loaded polymersomes were  
453 developed from a novel pegylated oleic acid polymer for sustained antibiotic delivery (Omolo et al.,  
454 2017). Overall, these works represent the proof-of-principle for the feasibility of choice of nanocarriers,  
455 as alternative drug delivery systems to obtain the desired drug release rates and bioavailability  
456 (Kalhapure et al., 2015). However, the effectiveness of those nanocarriers was seriously undermined by  
457 their poor ability to cross the *stratum corneum*, a skin barrier displaying low permeability unless proper  
458 exogenous physical stimuli are provided (Azagury et al., 2014; Park et al, 2012).

459 For these reasons, the present study aimed at developing Vm nanocarriers as a new platform to be  
460 effectively and safely employed for Vm topical administration to treat wound infections. To this  
461 purpose, NBs with core-shell nanostructures were identified as first choice carriers due to their known  
462 benefits in association with drug delivery, including small size, stability, suitability for drug loading,  
463 responsiveness to external stimuli such as US, and controlled drug release abilities (Marano et al.,  
464 2016; Cavalli et al., 2009a; Cavalli et al., 2009b; Cavalli et al., 2016). In this study, dextran sulfate was  
465 chosen as main constituent of the polysaccharidic shell as a consequence of the large amount of data  
466 from the literature supporting dextran biocompatibility (Bos et al., 2005; De Groot et al., 2001).  
467 Encouragingly, dextran-based hydrogels have already been employed as matrices in tissue engineering,  
468 without showing signs of inflammation *in vivo* (Möller et al., 2007), and recent toxicological studies  
469 have shown that dextran, as well as the products from its mechano-chemical processing, can be  
470 classified as class 4 (low-toxicity) substances (Dushkin et al., 2013). Moreover, dextran sulfate presents  
471 a negative charge that can electrostatically interact with the positive charged Vm. On the other hand,  
472 PFP was employed as principal constituent of the inner core, since it is the most widely used  
473 fluorocarbon in oxygenating emulsions and NB formulations (Cabralés and Intaglietta, 2013, Castro  
474 and Briceno, 2010). In order to load Vm, dextran sulfate-shelled/PFP-cored NBs were then  
475 functionalized by exploiting the electrostatic interactions occurring between the negatively charged  
476 sulfate groups of the shell and the protonated amino groups of the drug. The obtained VmLNBS  
477 displayed a spherical shape and a well-defined core-shell structure with a polymeric shell thickness of  
478 about 40 nm, average diameters of 300 nm, viscosity of 1.25 cP, and negatively charged surfaces. Of  
479 note, the observed decrease of zeta potential values of ~ 15 % for VmLNBS (around -29 mV) with  
480 respect to blank NBs (around -34 mV) confirmed the occurrence of electrostatic interactions between  
481 positive amino groups of the drug and negative sulfate groups of the polymer, leading to a partial

482 charge neutralization of the bubble surface and allowing a good Vm encapsulation efficiency (86%)  
483 and loading capacity (29%) in the NB systems.

484 In addition, it should be noticed that since the zeta potential measures charge repulsion or attraction  
485 between particles, it represents a fundamental parameter to avoid nanoparticle aggregation, with zeta  
486 potentials lower than -25 mV or larger than +25 mV being generally required for physical stability of  
487 colloid systems (Shah and Eldridge, 2014). The stability of VmLNB formulations was further  
488 confirmed by long-term checking of their size, surface charge, and viscosity values, which did not  
489 show any significant changes up to six months after manufacturing, stored at 4 °C. On the other hand,  
490 drug stability was comparatively checked between free Vm solution and VmLNB suspension either  
491 over time (up to 14 days) or at different temperatures (25°C and 37°C), revealing an increased stability  
492 for Vm when properly encapsulated in the nanocarriers. This appears as an undoubtedly advantageous  
493 feature for VmLNB formulations, since they might prove useful to overcome the reported instability of  
494 Vm in aqueous solutions at body temperature (Mawhinney et al., 1992, Raverdy ~~V~~-et al., 2013).

495 Interestingly, VmLNBs displayed a slow and prolonged drug release kinetics compared to Vm aqueous  
496 solution, with only 16% of the drug being released from VmLNBs after 6 h. These data support the  
497 hypothesis that VmLNBs may be employed as an effective drug reservoir until reaching the target site,  
498 where the antibiotic would be released upon sonication at an appropriate moment only. The features of  
499 VmLNBs might be exploited for the design of innovative wound dressing following their inclusion in  
500 polymeric base. Indeed, NBs can be dispersed in polymer gel without changing physico-chemical  
501 characteristics, as previously showed (Prato et al., 2015). Another intriguing feature of VmLNBs relies  
502 on the reported evidence that surface charges play a pivotal role in making a nanoparticle suitable for  
503 topical treatment, since they enhance its interaction with the skin and improve its therapeutic effect on  
504 inflamed cutaneous tissues, either without (Abdel-Mottaleb et al., 2012) or with concomitant US  
505 treatment (Lopez et al., 2011). Although cationic nanoparticles are generally preferred for topical

506 treatment due to the anionic nature of the skin (Wu et al., 2010), some authors have shown that anionic  
507 nanoparticles can be more effective (Lee et al., 2013) and less toxic (Ryman-Rasmussen et al., 2007)  
508 than the cationic ones. These latter data appear consistent with our results through investigation by  
509 biochemical assays to assess VmLNB biocompatibility with human skin tissues. Indeed, VmLNBs did  
510 not induce any *in vitro* cytotoxic effects on HaCaT keratinocytes, a skin cell line that was originally  
511 immortalized from a 62-year old donor (Boukamp et al., 1988). This peculiar information strengthens  
512 remarkably the evidence on VmLNB safety for future topical applications.

513 VmLNB and carrier-free Vm antimicrobial activity against MRSA were comparatively investigated,  
514 also analyzing Vm and NB physical interaction with the bacterial cell wall by confocal microscopy.  
515 Interestingly, VmLNBs were more effective in MRSA bacterial growth inhibition than free Vm,  
516 promoting enhanced and earlier antibacterial effects, although they were not internalized by bacteria,  
517 opposite to free Vm. This behavior appears to be a likely consequence of time-sustained release of Vm  
518 from VmLNBs.

519 Notably, an important issue that requires caution while evaluating the feasibility for any topical drug  
520 treatment is represented by the considerably low degree of permeability of the skin, the primary  
521 defense system for the body. This organ consists of several layers, including the *stratum corneum*, the  
522 epidermis, and the dermis. In particular the *stratum corneum* - composed of corneocytes interspersed in  
523 a laminate of compressed keratin and intercorneocyte lipid lamellae - is very poorly permeable to  
524 foreign molecules and represents the main obstacle to transdermal drug delivery (Naik et al., 2000).  
525 However, an ideal antibiotic drug formulation should be efficiently localized in the epidermis/dermis  
526 and provide a sustained drug release over time (Prabhu et al., 2012). To allow a drug to penetrate the  
527 skin, several approaches have been proposed, including skin patches, iontophoresis, chemical  
528 enhancers, and US-triggered sonophoresis (Park et al., 2014).

529 Interestingly, antimicrobial properties have been reported for US, although its effectiveness strongly  
530 varies depending on the targeted type of pathogen (fungi vs bacteria; cocci vs bacilli; Gram-positive vs  
531 Gram-negative) (Sango et al., 2014). Furthermore, synergistic effects between US and antibiotics have  
532 been reported in a series of studies: i) antibiotic treatment coupled with US irradiation resulted in  
533 enhanced bactericidal activity against both Gram-positive and Gram-negative bacteria, especially for  
534 aminoglycosides (Yu et al., 2012); ii) the combination of Vm and US decreased *S. aureus* viable counts  
535 by two orders of magnitude compared to Vm alone (Ayan et al., 2008); and iii) the addition of NB-  
536 enhanced US to doxycycline treatment improved the drug effectiveness in eradicating intracellular  
537 *Chlamydia trachomatis* (Ikeka-Dantsuji et al., 2011). US-dependent enhancement of antibiotic action  
538 on biofilms was named as a 'bioacoustic effect'. Interestingly, Vm transfer through *S. epidermidis*  
539 biofilms was shown to be significantly enhanced by US, with bubbles being able to increase the biofilm  
540 permeability to Vm (Dong ~~Y~~-et al., 2013).

541 As discussed previously, VmLNBS can be effectively employed as an important reservoir to store the  
542 drug until trespassing the *stratum corneum* of the skin and reaching the target site. In order to achieve  
543 the latter goal, US was assayed for its ability to induce VmLNBS to trespass an *in vitro* cutaneous layer,  
544 thereby releasing Vm throughout the skin. Notably, the skin from the pig ear is widely recognized as a  
545 good model for human skin permeability, since it displays human-like histological and physiological  
546 properties, including epidermal thickness and composition, dermal structure, lipid content and general  
547 morphology (Dick ~~and Scottet al.~~, 1992). The validity of the porcine model has been established by  
548 comparing the permeability of simple marker molecules with the corresponding values across human  
549 skin (Herkenne et al., 2006, Sekkat et al., 2002). Therefore, the porcine ear skin represents so far the  
550 most accountable *in vitro* model to mimic the human skin in studies on percutaneous penetration  
551 (Jacobi et al., 2007). In our experiments, US appeared essential to promote Vm release from VmLNBS  
552 throughout the pig skin layers, in line with previous reports on NBs and sonophoresis. On the contrary,

553 the passive transport of free vancomycin hydrochloride was negligible, being a charged and hydrophilic  
554 molecule. The amount of Vm accumulated in the skin after US application combined with NBs was  
555 greater than MIC value.

556

## 557 **5. Conclusions**

558 | In the present work, dextran sulfate-shelled and ~~PFP~~perfluoropentane-filled NBs were developed for  
559 Vm delivery. VLNBs proved to be effective in MRSA bacterial killing without showing toxic effects  
560 on human keratinocytes. The combination of NBs and US enhanced Vm permeation through pig skin  
561 and promoted drug skin accumulation. Based on these results, Vm topical administration through  
562 proper NB formulations might be a promising strategy for the local treatment of MRSA skin infections.  
563 The study represents the proof of concept for the future development of advanced multifunctional  
564 therapeutic systems to treat infected wounds.

565 **Acknowledgements**

566 The present work was supported by funds from University of Torino (ex 60% to RC and RS),  
567 Compagnia di San Paolo (ORTO11CE8R 2011 to CG and Torino\_call2014\_L2\_207 to AMC), and  
568 Fondazione Cariplo (HyWonNa project grant to MP). Thanks are due to Aurelio Malabaila for  
569 providing MRSA strain and to Giorgio Gribaudo for allowing to use his lab facilities to perform  
570 confocal microscopy studies.

571 .

572

573

574

575 **References**

576

577 Abdel-Mottaleb, M.M., Moulari, B., Beduneau, A., Pellequer, Y., Lamprecht, A., 2012. Surface-  
578 charge-dependent nanoparticles accumulation in inflamed skin. *J. Pharm. Sci.* 101, 4231-4239.

579

580 Ayan, İ., Aslan, G., Çömelekoğlu, Ü., Yılmaz, N., Çolak, M., 2008. The effect of low-intensity pulsed  
581 sound waves delivered by the Exogen device on *Staphylococcus aureus* morphology and genetics. *Acta*  
582 *orthopædica et traumatologica turcica* 42(4), 272-277.

583

584 Azagury, A., Khoury, L., Enden, G., Kost, J., 2014. Ultrasound mediated transdermal drug  
585 delivery. *Adv. drug del. rev.* 72, 127-143.

586

587 Banche, G., Prato, M., Magnetto, C., Allizond, V., Giribaldi, G., Argenziano, M., Khadjavi, A., Gulino,  
588 G.R., Finesso, N., Mandras, N., Tullio, V., Cavalli, R., Guiot, C., Cuffini, A.M., -2015. Antimicrobial  
589 chitosan nanodroplets: new insights for ultrasound-mediated adjuvant treatment of skin infection.  
590 *Future Microbiol.* 10(6), 929-939. doi: 10.2217/fmb.15.27. PubMed PMID: 26059617.

591

592 Basilio, N., Magnetto, C., D'Alessandro, S., Panariti, A., Rivolta, I., Genova, T., Khadjavi, A., Gulino,  
593 G.R., Argenziano, M., Soster, M., Cavalli, R., Giribaldi, G., Guiot, C., Prato, M., 2015. Dextran-  
594 shelled oxygen-loaded nanodroplets reestablish a normoxia-like pro-angiogenic phenotype and  
595 behavior in hypoxic human dermal microvascular endothelium. *Toxicol. Appl. Pharmacol.* 288(3), 330-  
596 338. doi: 10.1016/j.taap.2015.08.005. Epub 2015 Aug 12. PubMed PMID: 26276311.

597



598 Bos, G.W., Hennink, W.E., Brouwer, L.A., den Otter, W., Veldhuis, F.J., van Nostrum, C.F., van Luyn  
599 M.J., 2005. Tissue reactions of in situ formed dextran hydrogels crosslinked by stereocomplex  
600 formation after subcutaneous implantation in rats. *Biomaterials* 26, 3901–3909.

601

602 Boukamp, P., Dzarlieva-Petrusevska, R.T., Breitzkreuz, D., Hornung, J., Markham, A., Fusenig, N.E.,  
603 1988. Normal keratinization in a spontaneously immortalized aneuploid human keratinocyte cell line. *J.*  
604 *Cell. Biol.* 106, 761-771.

605

606 Cabrales, P., Intaglietta, M., 2013. Blood substitutes: evolution from noncarrying to oxygen- and gas-  
607 carrying fluids. *ASAIO J.* 59, 337-354.

608

609 Castro, C.I., Briceno, J.C., 2010. Perfluorocarbon-based oxygen carriers: review of products and trials.  
610 *Artif. Organs.* 34, 622-634.

611

612 Cavalli, R., Bisazza, A., Rolfo, A., Balbis, S., Madonnaripa, D., Caniggia, I., Guiot, C., 2009a.  
613 Ultrasound-mediated oxygen delivery from chitosan nanobubbles. *Int. J. Pharm.* 378, 215–217.

614

615 Cavalli, R., Bisazza, A., Giustetto, P., Civra, A., Lembo, D., Trotta, G., Guiot, C., Trotta, M., 2009b.  
616 Preparation and characterization of dextran nanobubbles for oxygen delivery. *Int. J. Pharm.* 381, 160-  
617 165.

618

619 Cavalli, R., Bisazza, A., Trotta, M., Argenziano, M., Civra, A., Donalisio, M., Lembo, D., 2012. New  
620 chitosan nanobubbles for ultrasound-mediated gene delivery: preparation and in vitro characterization.  
621 *Int. J. Nanomed.* 7, 3309-3318.

622

623 Cavalli, R., Bisazza, A., Lembo, D., 2013. Micro-and nanobubbles: A versatile non-viral platform for  
624 gene delivery. *Int. J. Pharm.* 456(2), 437-445.

625

626 Cavalli, R., Soster, M., Argenziano, M., 2016. Nanobubbles: a promising efficient tool for therapeutic  
627 delivery. *Ther. Deliv.* 7(2), 117-138. doi: 10.4155/tde.15.92. Epub 2016 Jan 15. PubMed PMID:  
628 26769397.

629

630 Clinical and Laboratory Standards Institute. Performance standards for antimicrobial susceptibility  
631 testing. Twenty-second informational supplement. Document M100-S22. Vol . 32, No. 3. Wayne, PA:  
632 CLSI; 2012.

633

634 Cumming, G., Fidler, F., Vaux, D.L., 2007. Error bars in experimental biology. *J Cell Biol.* 177, 7-11.

635

636 Daeschlein, G., 2013. Antimicrobial and antiseptic strategies in wound management. *Int. Wound J.*  
637 10(1), 9-14. doi: 10.1111/iwj.12175. Review. PubMed PMID:24251838.

638

639 De Groot C.J., Van Luyn, M.J.A., Van Dijk-Wolthuis, Cadée, J.A., Plantinga, J.A., Den Otter, W.,  
640 Hennink, W.E., 2001. In vitro biocompatibility of biodegradable dextran-based hydrogels tested with  
641 human fibroblast. *Biomaterials* 22, 1197–1203.

642

643 Delalande, A., Postema, M., Mignet, N., Midoux, P., Pichon, C., 2012. Ultrasound and microbubble-  
644 assisted gene delivery: recent advances and ongoing challenges. *Ther. Deliv.* 3, 1199-1215.

645

646 Dick, I.P., Scott, R.C. 1992. Pig ear skin as an in-vitro model for human skin permeability. *J. Pharm.*  
647 *Pharmacol.* 44, 640–645.

648

649 Diehr, P., O'Meara, E.S., Fitzpatrick, A., Newman, A.B., Kuller, L., Burke, G., 2008. Weight,  
650 mortality, years of healthy life, and active life expectancy in older adults. *J. Am. Geriatr. Soc.* 56(1),  
651 76-83. Epub 2007 Nov 20. PubMed PMID: 18031486; PubMed Central PMCID: PMC3865852.

652

653 Dong, Y., Chen, S., Wang, Z., Peng, N., Yu, J., 2013. Synergy of ultrasound microbubbles and  
654 vancomycin against *Staphylococcus epidermidis* biofilm. *J. Antimicrob. Chemother.* 68, 816-  
655 826.

656

657 Dushkin, A.V., Meteleva, E.S., Tolstikova, T.G., Pavlova, A.V., Khvostov, M.V. 2013. Gel  
658 chromatographic and toxicological studies of the mechanochemical transformations of water-soluble  
659 polysaccharides. *Pharm. Chem. J.* 46, 630-633.

660

661 Fokong, S., Theek, B., Wu, Z., Koczera, P., Appold, L., Jorge, S., Resch-Genger, U., VanZandvoort,  
662 M., Storm, G., Kiessling, F., Lammers, T., 2012. Image-guided, targeted and triggered drug delivery to  
663 tumors using polymer-based microbubbles. *J. Control. Rel.* 163, 75–81.

664

665 Giandalia, G., De Caro, V., Cordone, L., Giannola, L.I. 2001. Trehalose-hydroxyethylcellulose  
666 microspheres containing vancomycin for topical drug delivery. *Eur. J. Pharm. and Biopharm.: official*  
667 *journal of Arbeitsgemeinschaft fur Pharmazeutische Verfahrenstechnik e.V.* 52, 83-89.

668

669 Guiot, C., Pastore, G., Napoleone, M., Gabriele, P., Trotta, M., Cavalli, R., 2006. Thermal response of  
670 contrast agent microbubbles: preliminary results from physico-chemical and US-imaging  
671 characterization. *Ultrasonics*. 44(1), 127-130. Epub 2006 Jun 30. PubMed PMID: 17056082.

672

673 Gulino, G.R., Magnetto, C., Khadjavi, A., Panariti, A., Rivolta, I., Soster, M., Argenziano, M., Cavalli,  
674 R., Giribaldi, G., Guiot, C., Prato, M., 2015. Oxygen-Loaded Nanodroplets Effectively Abrogate  
675 Hypoxia Dysregulating Effects on Secretion of MMP-9 and TIMP-1 by Human Monocytes. *Mediators*  
676 *Inflamm.* 2015, 964838. doi: 10.1155/2015/964838. Epub 2015 Mar 23. PubMed PMID: 25878404;  
677 PubMed Central PMCID: PMC4386605.

678

679 Gurusamy, K.S., Koti, R., Toon, C.D., Wilson, P., Davidson, B.R., 2013. Antibiotic therapy for the  
680 treatment of methicillin-resistant *Staphylococcus aureus* (MRSA) infections in surgical wounds.  
681 *Cochrane Database Syst. Rev.* 20, 8:CD009726. doi: 10.1002/14651858.CD009726.pub2. Review.  
682 PubMed PMID: 23963687.

683

684 Herkenne, C., Naik, A., Kalia, Y.N., Hadgraft, J., Guy, R.H., 2006. Pig ear skin ex vivo as a  
685 model for in vivo dermatopharmacokinetic studies in man. *Pharm. Res.* 23, 1850-1856.

686

687 Ikeda-Dantsuji, Y., Feril, L. B., Tachibana, K., Ogawa, K., Endo, H., Harada, Y., Suzuki, R.,  
688 Maruyama, K., 2011. Synergistic effect of ultrasound and antibiotics against *Chlamydia trachomatis*-  
689 infected human epithelial cells in vitro. *Ultrasonics sonochemistry* 18(1), 425-430.

690

691 Jacobi, U., Kaiser, M., Toll, R., Mangelsdorf, S., Audring, H., Otberg, N., Sterry, W., Lademann, J.,  
692 2007. Porcine ear skin: an in vitro model for human skin. *Skin Research and Technology* 13(1), 19-24.

693

694 Karshafian, R., Bevan, P.D., Williams, R., Samac, S., Burns, P.N., 2009. Sonoporation by ultrasound-  
695 activated microbubble contrast agents: effect of acoustic exposure parameters on cell membrane  
696 permeability and cell viability. *Ultrasound Med. Biol.* 35, 847-860.

697

698 Khadjavi, A., Magnetto, C., Panariti, A., Argenziano, M., Gulino, G.R., Rivolta, I., Cavalli, R.,  
699 Giribaldi, G., Guiot, C., Prato, M., 2015. Chitosan-shelled oxygen-loaded nanodroplets abrogate  
700 hypoxia dysregulation of human keratinocyte gelatinases and inhibitors: New insights for chronic  
701 wound healing. *Toxicol. Appl. Pharmacol.* 286(3), 198-206. doi: 10.1016/j.taap.2015.04.015. Epub  
702 2015 Apr 30. PubMed PMID: 25937238.

703

704 Kalhapure, R.S., Suleman, N., Mocktar, C., Seedat, N., Govender, T., 2015. Nanoengineered Drug  
705 Delivery Systems for Enhancing Antibiotic Therapy. *J. Pharm. Sci.* 104, 872–905.

706

707 Khangtragool, A., Ausayakhun, S., Leesawat, P., Laokul, C., Molloy, R., 2011. Chitosan as an ocular  
708 drug delivery vehicle for vancomycin. *J. App. Pol. Sci.* 122, 3160-3167.

709

710 Koyama, N., Inokoshi, J., Tomoda, H., 2012. Anti-infectious agents against MRSA. *Molecules* 18(1),  
711 204-224. doi: 10.3390/molecules18010204.

712

713 Kullar, R., Sakoulas, G., Deresinski, S., van Hal, S. J., 2016~~5~~. When sepsis persists: a review of MRSA  
714 bacteraemia salvage therapy. *J. Antimicrob. Chemother.* 71, 576-~~5~~86.

715

Formatted: English (United States)

Formatted: English (United States)

Formatted: English (United States)

716 Lazarus, G.S., Cooper, D.M., Knighton, D.R., Percoraro, R.E., Rodeheaver, G., Robson, M.C., 1994.  
717 Definitions and guidelines for assessment of wounds and evaluation of healing. *Wound Repair Regen.*  
718 2(3), 165-170. PubMed PMID: 17156107.  
719

720 Lee, O., Jeong, S.H., Shin, W.U., Lee, G., Oh, C., Son, S.W., 2013. Influence of surface charge of gold  
721 nanorods on skin penetration. *Skin Res. Technol.* 19, e390-e396.  
722

723 Lopez, R.F., Seto, J.E., Blankschtein, D., Langer, R., 2011. Enhancing the transdermal delivery of rigid  
724 nanoparticles using the simultaneous application of ultrasound and sodium lauryl sulfate. *Biomaterials.*  
725 32, 933-941.  
726

727 Magnetto, C., Prato, M., Khadjavi, A., Giribaldi, G., Fenoglio, I., Jose, J., Gulino, G.R., Cavallo, F.,  
728 Quaglino, E., Benintende, E., Varetto, G., Troia, A., Cavalli, R., Guiot, C., 2014. Ultrasound-activated  
729 decafluoropentane-cored and chitosan-shelled nanodroplets for oxygen delivery to hypoxic cutaneous  
730 tissues. *RSC Advances* 4, 38433-38441.  
731

732 Marano, F., Argenziano, M., Frairia, R., Adamini, A., Bosco, O., Rinella, L., Fortunati, N., Cavalli, R.,  
733 Catalano, M.G., 2016. Doxorubicin-Loaded Nanobubbles Combined with Extracorporeal Shock  
734 Waves: Basis for a New Drug Delivery Tool in Anaplastic Thyroid Cancer. *Thyroid* 26(5), 705-716  
735

736 Markova, A., Mostow, E.N., 2012. US skin disease assessment: ulcer and wound care. *Dermatol. Clin.*  
737 30(1), 107-111. ix. doi: 10.1016/j.det.2011.08.005. Review. PubMed PMID: 22117872.  
738

739 Marxer, E.E.J., Brüßler, J., Becker, A., Schümmelfeder, J., Schubert, R., Nimsky, C., Bakowsky, U.,  
740 2011. Development and characterization of new nanoscaled ultrasound active lipid dispersions as  
741 contrast agents. *Eur. J. Pharm. Biopharm.* 77, 430–437.  
742

743 Mawhinney, W.M., Adair, C.G., Gorman, S.P., McClurg, B., 1992. Stability of vancomycin  
744 hydrochloride in peritoneal dialysis solution. *Am. J. Hosp. Pharm.* 49(1), 137-139. PubMed PMID:  
745 1570857.  
746

747 Möller, S., Weisser, J., Bischoff, S., Schnabelrauch, M., 2007. Dextran and hyaluronan methacrilate  
748 based hydrogels as matrices for soft tissue reconstruction. *Biomol. Eng.* 24, 496–504.  
749

750 Muppidi, K., Wang, J., Betageri, G., Pumerantz, A.S. 2011. PEGylated liposome encapsulation  
751 increases the lung tissue concentration of vancomycin. *Antimicrob. Agents Chemother.* 55(10), 4537-  
752 4542.  
753

754 Naik, A., Kalia, Y.N., Guy, R.H., 2000. Transdermal drug delivery: overcoming the skin's barrier  
755 function. *Pharm. Sci. Technol. Today.* 3, 318–326.  
756

757 Omolo, C.A., Kalhapure, R.S., Jadhav, M., Rambharose, S., Mocktar, C., Ndesendo, V.M., Govender,  
758 T. 2017. PEGylated oleic acid: A promising amphiphilic polymer for nano-antibiotic delivery. *Eur. J.*  
759 *Pharm. Biopharm.* 112, 96-108.  
760

761 Park, D., Ryu, H., Kim, H.S., Kim, Y.S., Choi, K.S., Park, H., Seo J., 2012. Sonophoresis Using  
762 Ultrasound Contrast Agents for Transdermal Drug Delivery: An In Vivo Experimental Study.  
763 *Ultrasound Med. & Biol.* 38(4), 642-650.  
764

765 Park, D., Park, H., Seo, J., Lee, S., 2014. Sonophoresis in transdermal drug delivery. *Ultrasonics*. 54,  
766 56-65.  
767

768 Payne, W.G., Naidu, D.K., Wheeler, C.K., Barkoe, D., Mentis, M., Salas, R.E., Smith, D.J., Robson,  
769 M.C., 2008. Wound healing in patients with cancer. *Eplasty*. 8, e9. PubMed PMID: 18264518; PubMed  
770 Central PMCID: PMC2206003.  
771

772 Pornpattananankul, D., Zhang, L., Olson, S., Aryal, S., Obonyo, M., Vecchio, K., Huang, C.M.,  
773 Zhang, L., 2011. Bacterial toxin-triggered drug release from gold nanoparticle-stabilized liposomes for  
774 the treatment of bacterial infection. *J. American Chem. Soc.*133(11), 4132-4139.  
775

776 Prabhu, P., Patravale, V., Joshi, M., 2012. Nanocarriers for effective topical delivery of anti-infectives.  
777 *Current Nanoscience* 8, 491-503.  
778

779 Prato, M., Magnetto, C., Jose, J., Khadjavi, A., Cavallo, F., Quaglino, E., Panariti, A., Rivolta, I.,  
780 Benintende, E., Varetto, G., Argenziano, M., Troia, A., Cavalli, R., Guiot C., 2015. 2H,3H-  
781 decafluoropentane-based nanodroplets: new perspectives for oxygen delivery to hypoxic cutaneous  
782 tissues. *Plos One* 10(3), e0119769. doi:10.1371/journal.pone.0119769  
783



784 Prato, M., Khadjavi, A., Magnetto, C., Gulino, G.R., Rolfo, A., Todros, T., Cavalli, R., Guiot, C., 2016.  
785 Effects of oxygen tension and dextran-shelled/2H,3H-decafluoropentane-cored oxygen-loaded  
786 nanodroplets on secretion of gelatinases and their inhibitors in term human placenta. *Biosci Biotechnol*  
787 *Biochem.* 80(3), 466-472. doi: 10.1080/09168451.2015.1095068. Epub 2015 Nov 2. PubMed PMID:  
788 26523859.

789

790 Price, M., 2010. Community-acquired methicillin-resistant *Staphylococcus aureus*: an ongoing  
791 challenge for WOC nursing. *J Wound Ostomy Continence Nurs.* 37(6), 633-638. doi:  
792 10.1097/WON.0b013e3181feb001. Review. PubMed PMID: 21076263.

793

794 Raverdy V., Ampe, E., Hecq, J.D., Tulkens, P. M., 2013. Stability and compatibility of vancomycin for  
795 administration by continuous infusion. *J. Antimicrob. Chemother.* 68, 1179-1182.

796

797 Ryman-Rasmussen, J.P., Riviere, J.E., Monteiro-Riviere, N.A., 2007. Surface coatings determine  
798 cytotoxicity and irritation potential of quantum dot nanoparticles in epidermal keratinocytes. *J Invest*  
799 *Dermatol.* 127, 143-153.

800

801 Sango, D.M., Abela, D., McElhatton, A., Valdramidis, V.P., 2014. Assisted ultrasound applications for  
802 the production of safe foods. *J. Appl. Microbiol.* 116, 1067-1083.

803

804 Sekkat, N., Kalia, Y.N., Guy, R.H., 2002. Biophysical study of porcine ear skin in vitro and its  
805 comparison to human skin in vivo. *J. Pharm. Sci.* 91, 2376-2381.

806 Shah, R., Eldridge, R., 2014. Optimisation and Stability Assessment of Solid Lipid Nanoparticles using  
807 Particle Size and Zeta Potential. *J. Phys. Sci.* 25, 59–75

808

809 Sharma, A., Arya, D.K., Dua, M., Chhatwal, G.S., Johri, A.K., 2012. Nano-technology for targeted  
810 drug delivery to combat antibiotic resistance. *Expert Opinion Drug Del.* 9, 1325-1332.

811

812 Vandecasteele, S.J., De Vriese, A.S., Tacconelli, E., 2012. The pharmacokinetics and  
813 pharmacodynamics of vancomycin in clinical practice: evidence and uncertainties. *J. Antim. Chem.* 68,  
814 743-748.

815

816 Vidal, C., González Quintela, A., Fuente, R., 1992. Toxic epidermal necrolysis due to vancomycin.  
817 *Ann Allergy.* 68(4), 345-347. PubMed PMID: 1558331.

818

819 Wu, X., Landfester, K., Musyanovych, A., Guy, R.H., 2010. Disposition of charged nanoparticles after  
820 their topical application to the skin. *Skin Pharmacol Physiol.* 23, 117-123.

821

822 Yin, T., Wang, P., Li, J., Wang, Y., Zheng, B., Zheng, R., Cheng, D., Shuai, X., 2014. Tumor-  
823 penetrating codelivery of siRNA and paclitaxel with ultrasound-responsive nanobubbles hetero-  
824 assembled from polymeric micelles and liposomes. *Biomaterials* 35(22), 5932-5943.

825

826 Yu, H., Chen, S., Cao, P., 2012. Synergistic bactericidal effects and mechanisms of low intensity  
827 ultrasound and antibiotics against bacteria: a review. *Ultrasonics sonochemistry* 19(3), 377-382.

828

829 Zilberman, M., Elsner, J.J., 2008. Antibiotic-eluting medical devices for various applications. *J Control*  
830 *Release* 130(3), 202-215. doi: 10.1016/j.jconrel.2008.05.020. Epub 2008 Aug 6. Review. PubMed  
831 PMID: 18687500.

832 **Figure legends**

833

834 **Figure 1. Schematic structure of VmLNB formulations.** Vm nanocarriers described in the present  
835 work display a core-shell structure. PFP was employed as core fluorocarbon, whereas dextran sulfate  
836 was chosen as polysaccharidic shell molecule. Vm was inserted into the outer shell throughout dextran  
837 sulfate chains. In selected experiments, VmLNBS were further functionalized by including fluorescent  
838 6-coumarin in the inner core.

839

840 **Figure 2. NB and VmLNB morphology.** NBs and VmLNBS were checked for morphology by TEM.  
841 Results are shown as representative images from three different preparations. Panel A. NB image by  
842 TEM. Panel B. VmLNB image by TEM. [\(see also Figure S1 in Supplementary Materials for additional](#)  
843 [images of multiple nanobubbles within the same field\).](#)

844

845 **Figure 3. Stability of Vm and VmLNB formulations.** The stability of Vm solution and VmLNB  
846 suspension was monitored up to 14 days either at room temperature (Panel A) or at 37°C (Panel B)  
847 through analysis by HPLC. Results are shown as means  $\pm$  SD from three different preparations for each  
848 formulation. Data were also analyzed for significance by ANOVA. Versus Vm solution: \*  $p < 0.001$ .

849

850 **Figure 4. Biocompatibility of Vm and VmLNBS with human keratinocytes *in vitro*.** HaCaT cells  
851 ( $10^6$  cells/2 mL DMEM medium implemented with 10% FCS) were left untreated (ctr) or treated with  
852 200 ~~micro~~uL of Vm solution or VmLNB suspension for 24 h in normoxia (20% O<sub>2</sub>). Thereafter, Vm  
853 and VmLNB cytotoxicity were measured through LDH assay (Panel A), whereas cell viability was  
854 measured through MTT assay (Panel B). Results are shown as means  $\pm$  SEM from three independent

855 experiments. Data were also evaluated for significance by ANOVA. No significant differences were  
856 found among all conditions.

857 **Figure 5. *In vitro* Vm release from Vm and VmLNB formulations.** Vm release from Vm solution  
858 and VmLNB suspension was monitored up to 6 h. Results are shown as means  $\pm$  SD from three  
859 different preparations for each formulation. Data were also analyzed for significance by ANOVA.  
860 Versus Vm solution: \*  $p < 0.001$ .

861

862 **Figure 6. Antibacterial activity of Vm and VmLNBS against MRSA.** MRSA were left for 2, 3, 4, 6  
863 and 24 hours at 37°C alone (ctr) or incubated with 10% v/v NBs or different concentrations of Vm,  
864 either free or loaded on VmLNBS (Panel A: 1 mg/mL; Panel B: 0.1 mg/mL; Panel C: 0.01 mg/mL;  
865 Panel D: 0.004 mg/mL). Results are shown as means  $\pm$  SEM from three independent experiments. Data  
866 on Vm- and VmLNB-treated samples were normalized upon Vm/VmLNB release ratios reported in  
867 Table [23](#) (see also in Supplementary Materials: Table [S34](#) for further information on percentages of  
868 drug release from VmLNBS at different times/concentrations; and Figure [S24](#) for raw data on VmLNB  
869 antibacterial effects). All data were also evaluated for significance by ANOVA. Versus ctr: \*  $p < 0.02$ ;  
870 versus Vm: °  $p < 0.05$ .

871

872 **Figure 7. Drug loading on dextran sulfate-shelled NBs prevents Vm internalization by MRSA.**  
873 MRSA were left alone or incubated with 10% v/v 6-coumarin-labeled VLNBS, 6-coumarin-labeled  
874 NBs, and FITC-labeled Vm for 2h at 37°C. After staining bacteria with PI, confocal fluorescent images  
875 were taken using FITC and TRITC filters. Data are shown as representative images from three  
876 independent experiments. Magnification: 100X. Red: PI. Green: 6-coumarin or FITC.

877

878 **Figure 8. US-triggered sonophoresis of VmLNBS through skin membranes.** US (t = 10 min; f = 2.5  
879 MHz; P = 5 W) abilities to induce sonophoresis and Vm permeation from VmLNBS were evaluated up  
880 to 6 h by using a vertical diffusion Franz cell consisting in two chambers (donor and recipient,  
881 respectively) separated by a pig skin layer (see scheme in Panel A). Results are shown in Panel B as  
882 means  $\pm$  SD from three independent experiments. Data were also evaluated for significance by  
883 ANOVA. Versus without US:  $p < 0.001$ .

884 **Tables and legends**

885

Formulation	Average diameter ± SD (nm)	Polydispersity index	Zeta Potential ± SD (mV)	<u>Viscosity</u> <u>(cP)</u>
NBs	313.4 ± 26.4	0.24 ± 0.02	- 34.5 ± 0.38	<u>1.22</u>
VmLNBS	304.6 ± 14.6	0.22 ± 0.03	- 28.6 ± 1.34	<u>1.25</u>
Fluorescent NBs	312.8 ± 22.7	0.25 ± 0.02	- 34.1 ± 1.22	<u>1.24</u>
Fluorescent VmLNBS	308.9 ± 22.4	0.23 ± 0.01	- 29.5 ± 1.88	<u>1.23</u>

Formatted Table

886

887 **Table 1. Physical-chemical characterization of NBs and VmLNBS.** Liquid formulations were  
 888 characterized for average diameters, polydispersity index, and zeta potential by light scattering. The  
 889 viscosity (cP) of NB and VmLNB suspensions was determined at 25 °C by using a Ubbelohde capillary  
 890 viscosimeter. Results are shown as means ± SD from three preparations. See also Figures 1-2 for  
 891 further detail on NB and VmLNB structure and morphology.

892

<del>Sample solution</del>	<del>Viscosity (cP)</del>
<del>Vm-</del>	<del>0.98</del>
<del>NBs</del>	<del>1.12</del>
<del>VmLNBS</del>	<del>1.25</del>

893

894 ~~**Table 2. Viscosity of Vm solution, NB, and VmLNB suspensions.** The viscosity (cP) of NB and~~  
 895 ~~VmLNB suspensions as well as free Vm solution was determined at 25 °C by using a Ubbelohde~~  
 896 ~~capillary viscosimeter. The results are reported in the table.~~

897

898

time (hours)	% drug release from Vm solution	% drug release from VmLNBs	Vm/VmLNB drug release ratio
2	36.57	5.99	6.11
3	45.97	7.97	5.78
4	57.16	10.27	5.57
6	73.44	14.59	5.03
24	92.34	35.84	2.58

899

900 **Table 23. *In vitro* drug release from Vm solution and VmLNB suspension.** After incubation for  
901 increasing times (first column), the percentages of *in vitro* drug release from Vm solution (second  
902 column) and VmLNB suspension (third column) were measured. Then, Vm/VmLNB drug release  
903 ratios (fourth column) were calculated for each time considered. All incubation times (2, 3, 4, 6, and  
904 24 h) were purposely chosen to further normalize the results from the experiments with MRSA (see  
905 Figure 6). Results are shown as mean values from three different preparations for each formulation.





Figure 2

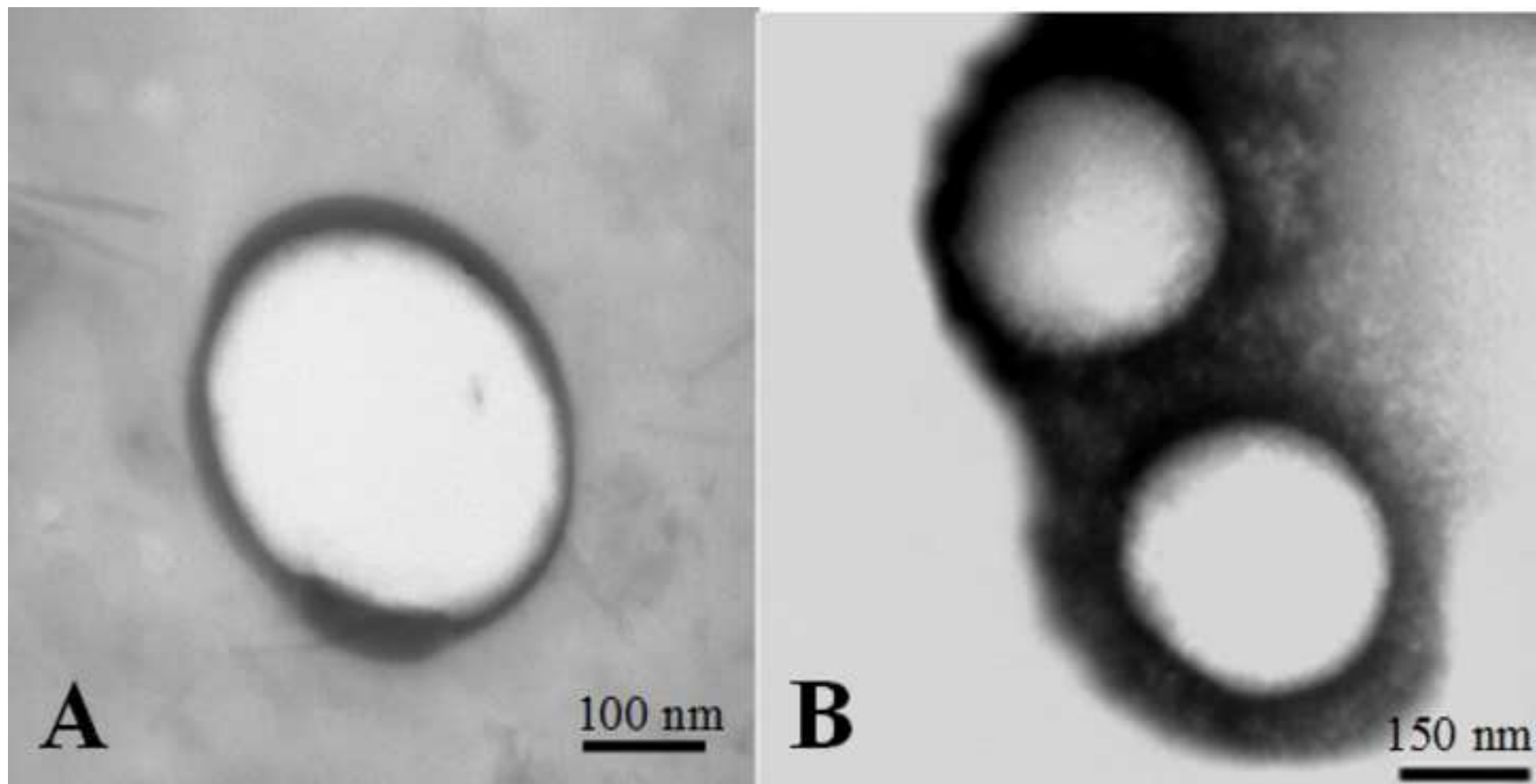


Figure 3

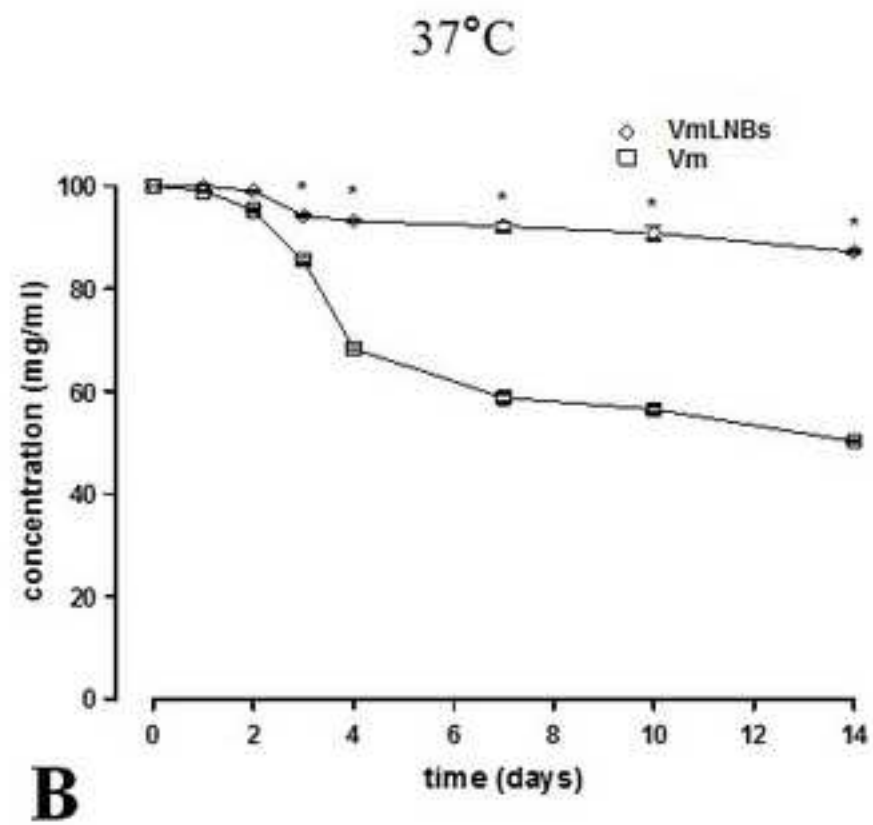
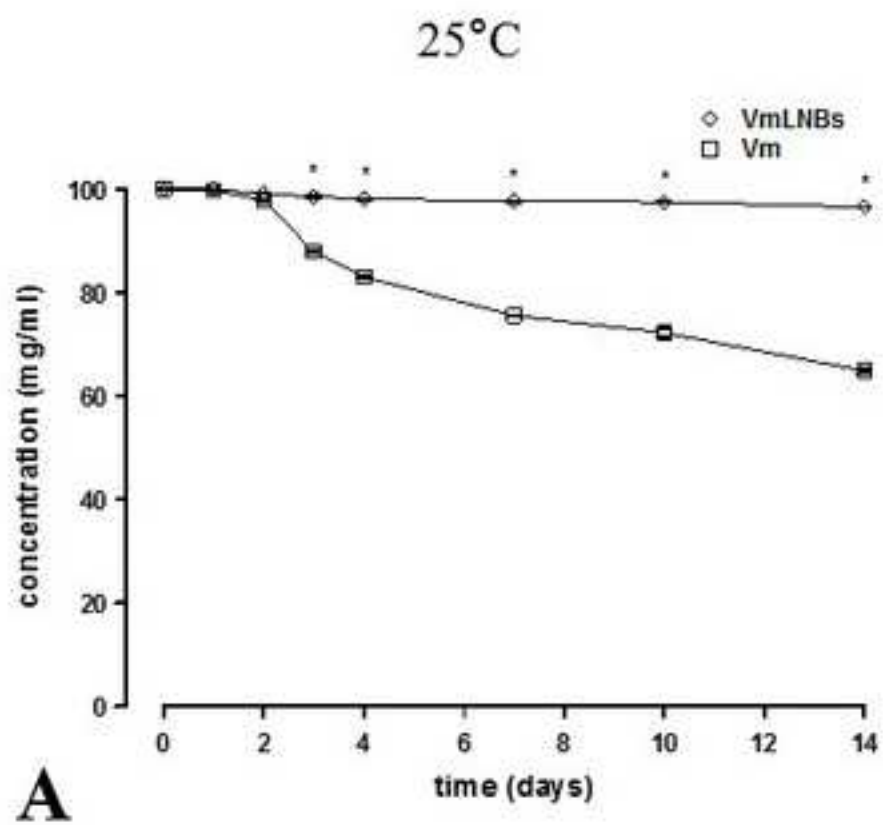


Figure 4

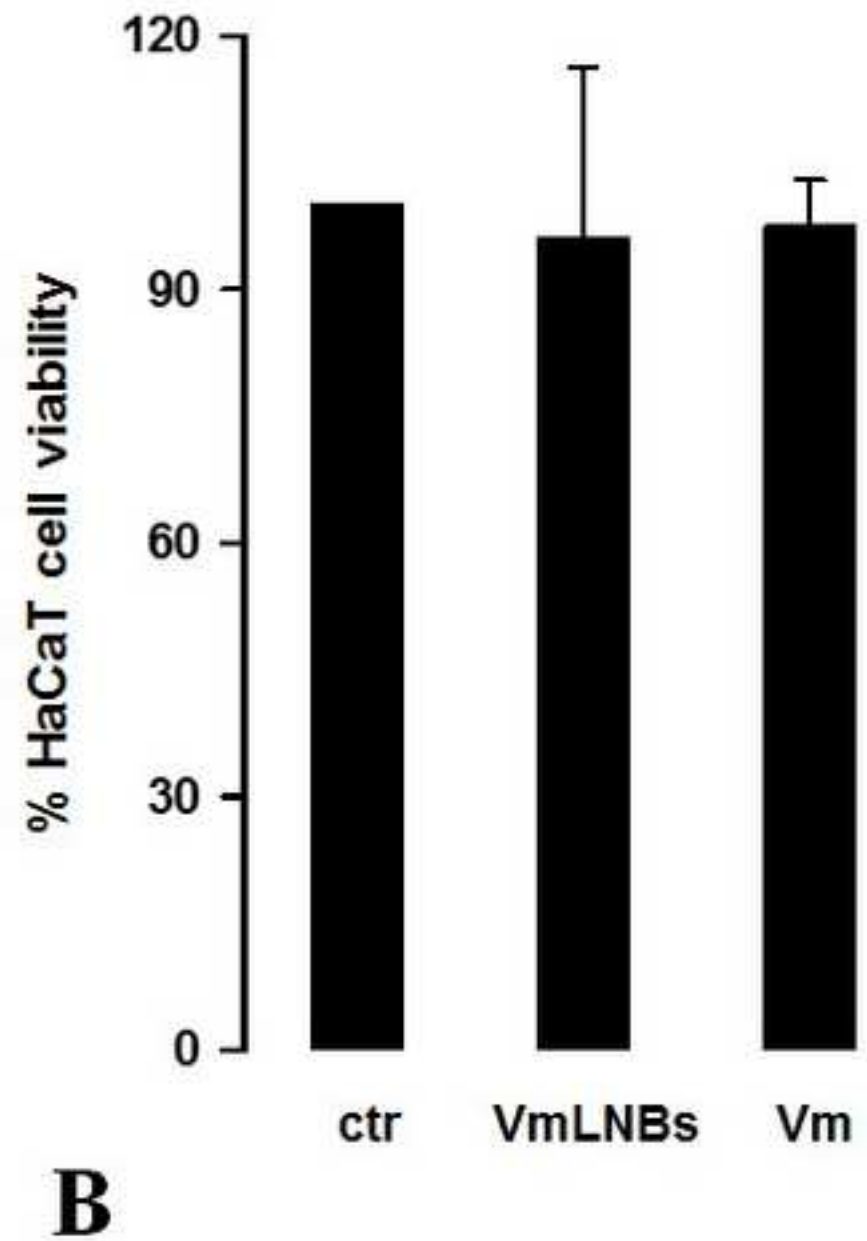
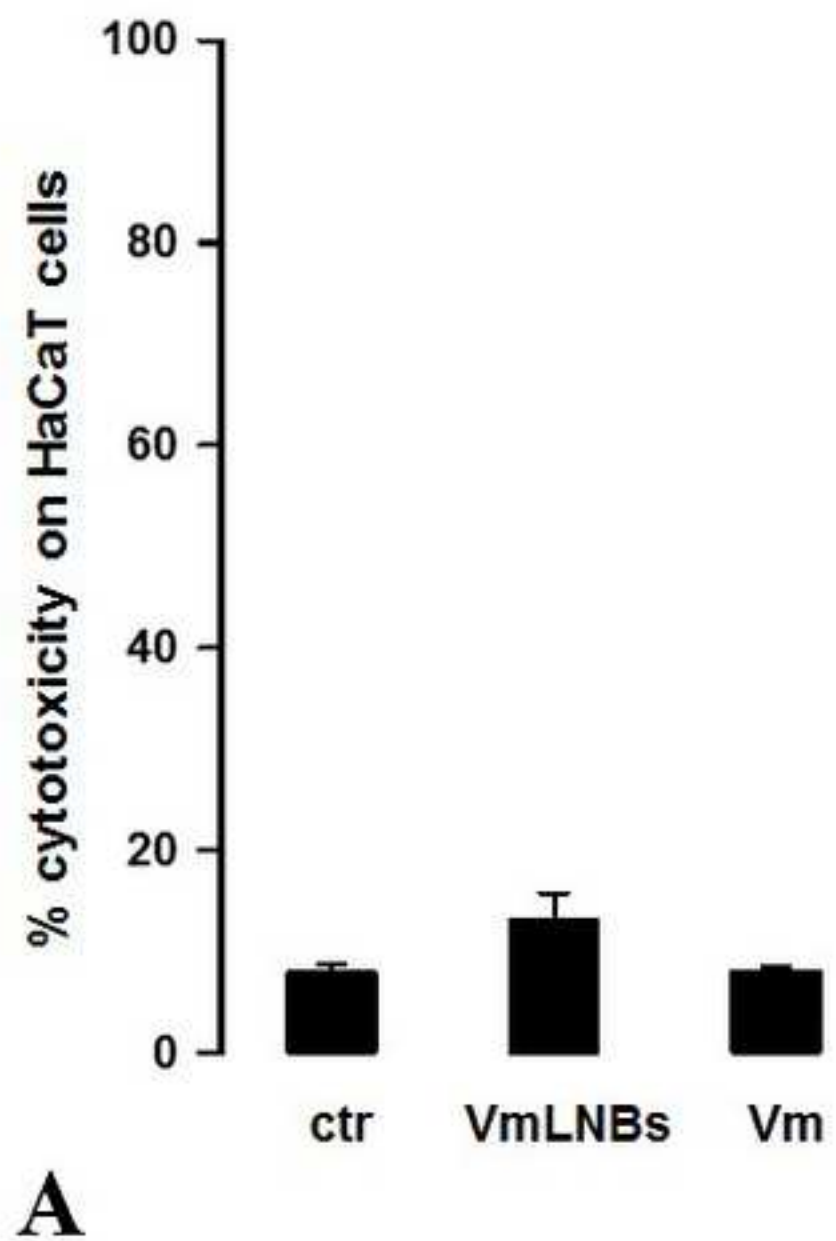


Figure 5

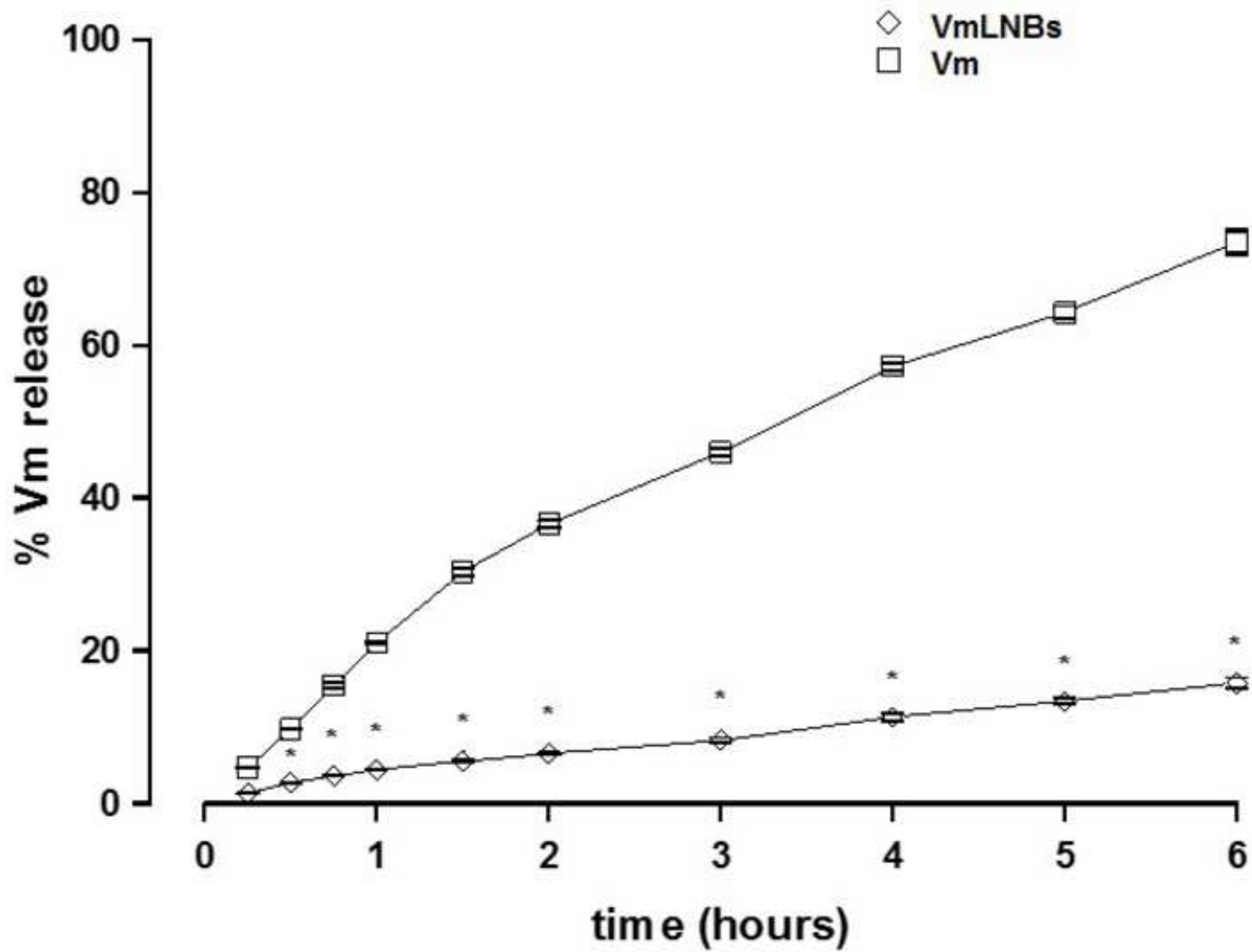


Figure 6

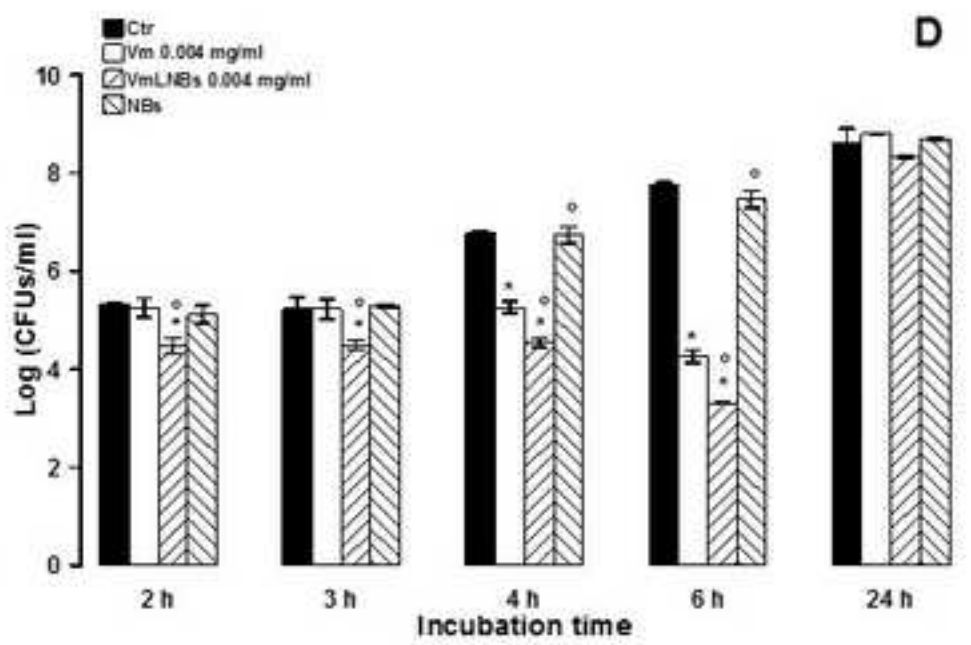
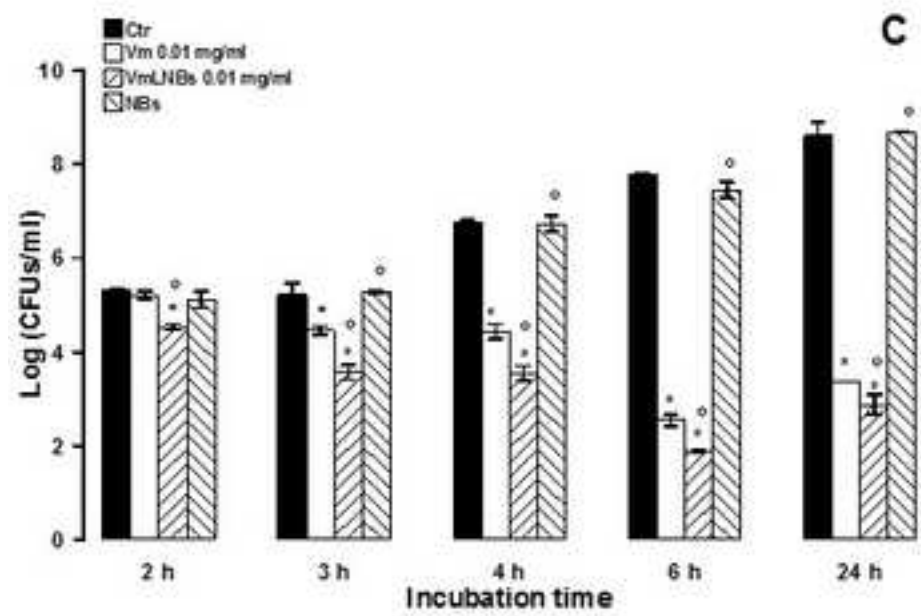
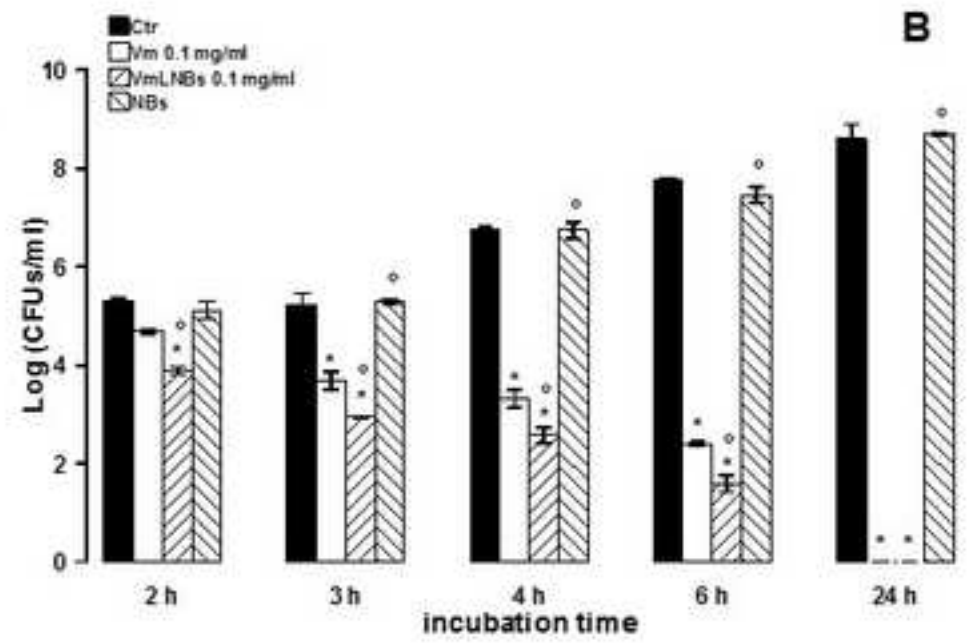
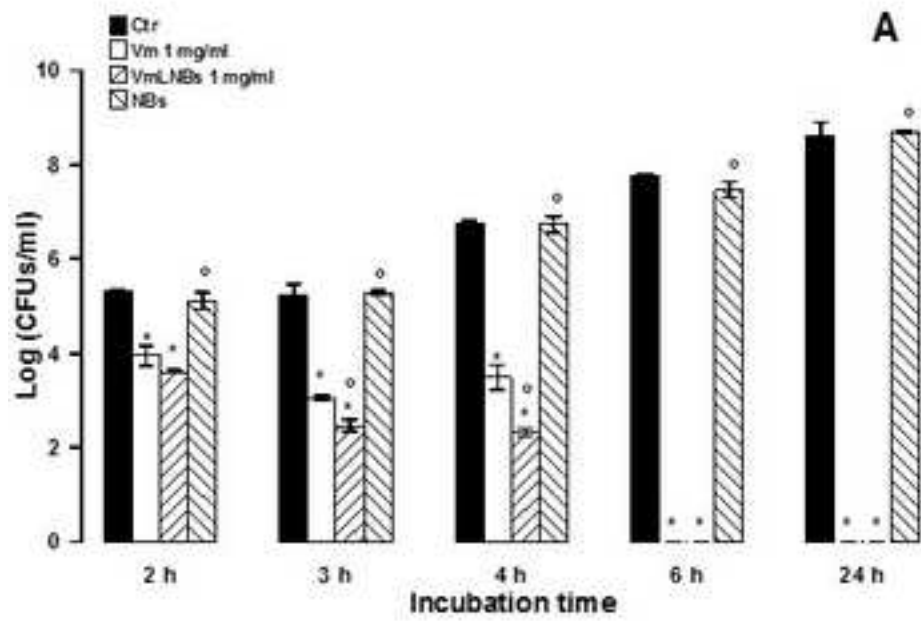


Figure 7

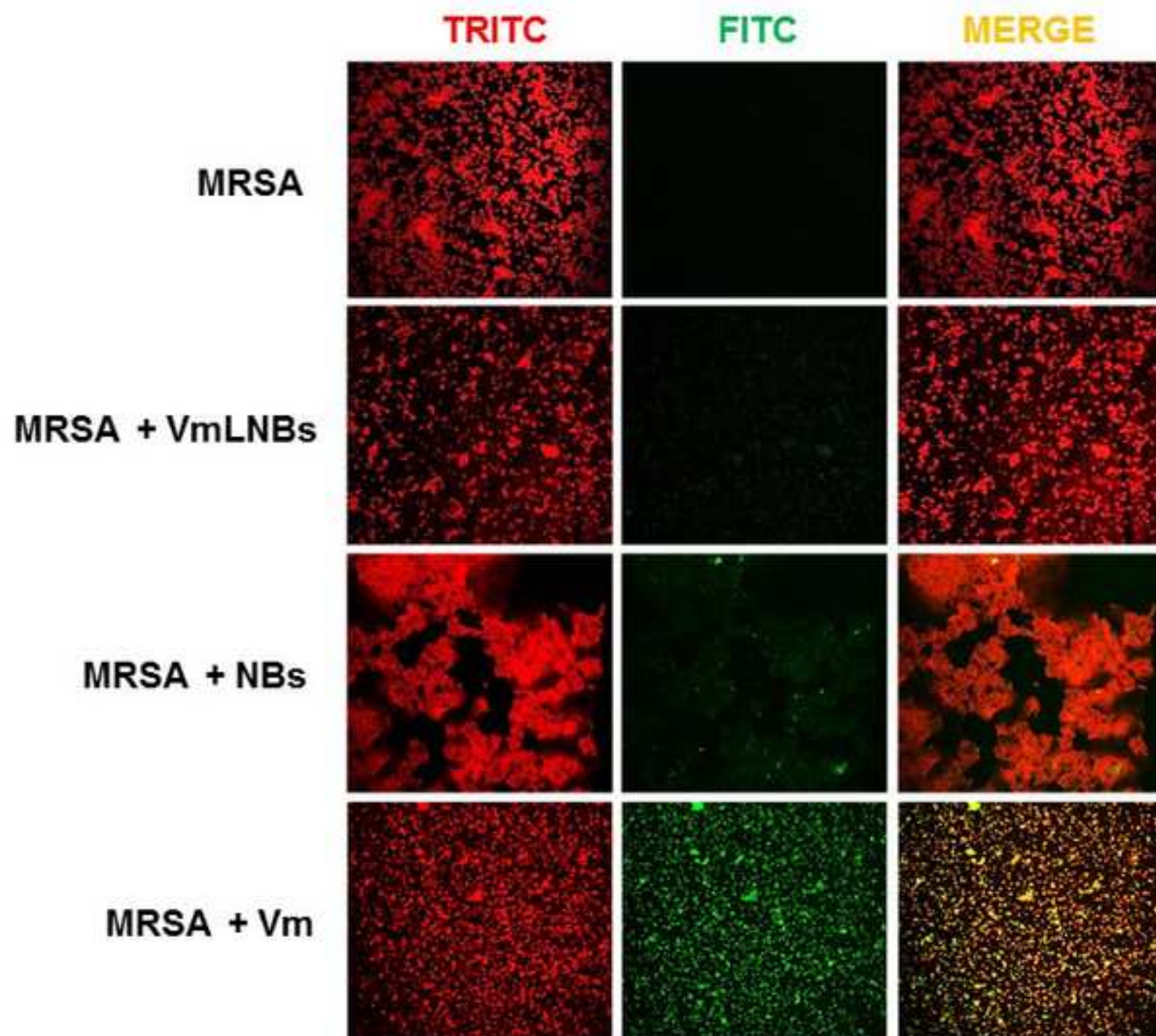
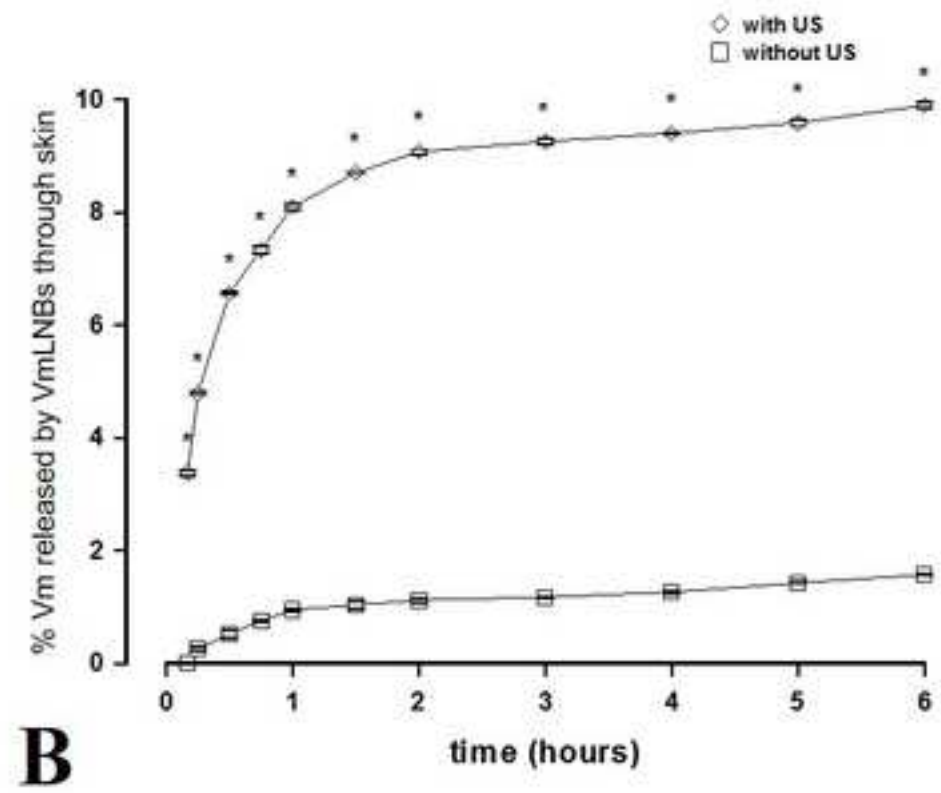
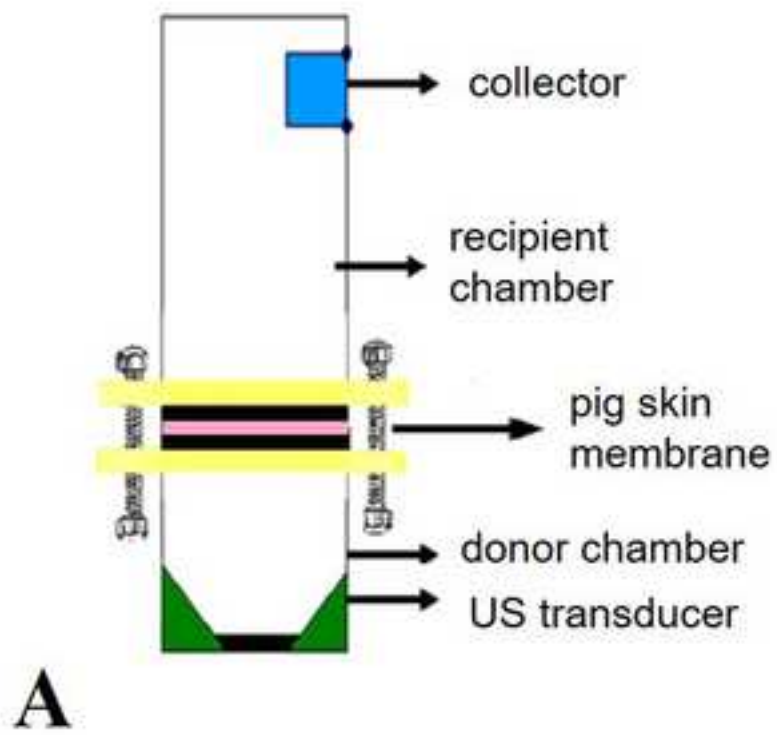


Figure 8



**Supplementary Material (clean copy)**

[Click here to download Supplementary Material: Argenziano et al Int J Pharm 2017 SUPPL MAT revised \(CLEAN COPY\).doc](#)



**Supplementary Material (marked copy)**

[Click here to download Supplementary Material: Argenziano et al Int J Pharm 2017 SUPPL MAT revised \(MARKED COPY\).doc](#)